Freie Universität Berlin

Institute of Chemistry and Biochemistry

Optical Spectra of Molecules Embedded in Helium Nanodroplets

BACHELOR'S THESIS
submitted by

Lasfitri Rosanty Sinaga
on 27th February 2018
Student number: 4625536

and written at
The Fritz-Haber Institute of the Max Planck Society

Examiner 1: Prof. Dr. Bretislav Friedrich
Examiner 2: Prof. Dr. Beate Paulus

Kurzfassung

Wir zeigen Simulationen und Anpassung der feldfreien und Stark optischen Spektren verschiedener Molekülarten in der Gasphase und in Heliumtröpfchen, die in der Literatur verfügbar sind, unter Verwendung eines Simulationsprogrammpakets PGOPHER. Weiterhin analysieren wir die relativen spektralen Breiten der feldfreien linearen und symmetrischen Top-Rotoren und zeigen eine Skalierungsbeziehung zwischen den relativen Spektralbreiten und den Renormalisierungsverhältnissen der Rotationskonstanten.

Abstract

We present simulations and fits of the field-free and Stark optical spectra of various types of molecules in the gas phase and in helium droplets that are available in the literature using a simulation package PGOPHER. Furthermore, we analyze the relative spectral widths of field free linear and symmetric top rotors and present a scaling relationship between the relative spectral widths and the renormalization ratios of the rotational constants.

Index

1. Introduction

Helium nanodroplets serve as cold superfluid matrices of a uniform temperature of 370 mK that cool all the degrees of freedom of the molecules doped into them. As a result, fewer states of the dopant species are populated than under thermal conditions or even in supersonic molecular beams and their spectra are less congested as a result. Moreover, many molecular species undergo a nearly-free rotation in the superfluid environment of the He droplets, which affords spectroscopic observation of their rotational transitions, apart from the elucidation of vibrational and electronic transitions. In addition, the spectroscopic investigation of molecules embedded in He droplets allows the study of solvation in a prototypical quantum liquid.

Helium is the only element that remains liquid at ambient pressure at temperatures down to the absolute zero. [1-7] Below the critical temperature, $T_c = 2.17$ K, the isotope ^{4}He becomes superfluid. It is the superfluidity of He droplets that enables the nearly-free rotation of the embedded species (often termed *impurities*).

In analogy with solid matrices, He droplets can act like nano-cryostats that stabilize short-lived unstable species and make their spectroscopic investigation possible. Helium droplets also allow for the formation of molecular complexes via multiple doping with atomic or molecular species: the van der Waals attraction between such species within a He droplet exceeds the attraction between either species and the He atoms that make up the droplet. Moreover, the cross section for the formation of a molecular complex is largely given by the size of the host droplet (typically comprised of 10^2 to 10^8 He atoms) and not the molecules that are to constitute the complex. Consequently, almost any molecular complex can be created by such a "synthesis" in He droplets.

This thesis is organized as follows: Chapter 2 begins with the fundamentals of helium nanodroplet spectroscopy and explores the concept of homogeneous and inhomogeneous broadening of spectral lines. Subsequently, the angulon treatment of a rotating quantum impurity is outlined. In Chapter 3, the simulation of rotationally resolved molecular spectra is discussed and the package PGOPHER presented. [8] Also discussed are the definitions of spectral-width and relative spectral-width. Chapter 4 begins by presenting our simulations and fits of the field-free and Stark rotational spectra of various types of molecules in the gas phase and in helium droplets that are

available in the literature. These serve to validate our calculations. Finally, we present the key result of this thesis, namely a scaling relationship between the relative spectral widths and the renormalization ratios of the rotational constants.

2. State of the art

In this chapter, a brief description of the state of the art of helium nanodroplet spectroscopy pertaining to the objectives of this thesis is provided. Beginning with the properties of superfluid helium, we explore the key ideas behind the Helium Nanodroplet Isolation (HENDI) technique for the spectroscopy of molecules.

2.1 Superfluid helium as a quantum matrix

Helium is the lightest noble gas that has nine known isotopes, two of which, ^{3}He and ^{4}He, are stable and occur in nature in the ratio of about 1 to 10^6. At a pressure of 1 bar and temperature below 2.17 K, ^{4}He undergoes a phase transition into a *superfluid* state. For ^{3}He, this transition occurs at 0.0025 K. [9] Before discussing superfluidity of helium, we first answer the question: What is superfluidity in general?

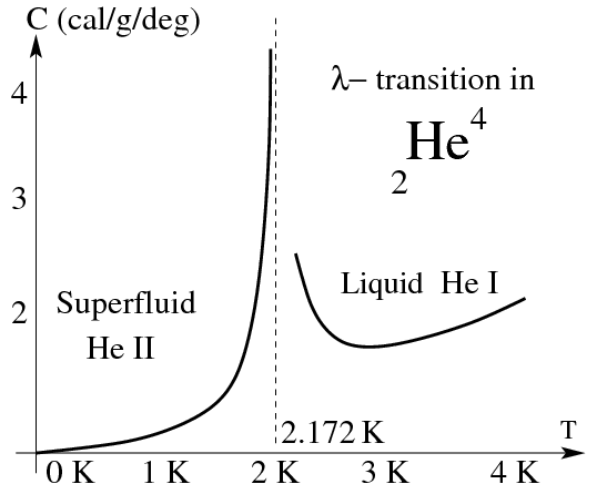

Fig. 2.1. Lambda transition of ^{4}He. [10] The dependence of the heat capacity C on temperature resembles the Greek letter λ, so the phase transition was dubbed a λ (lambda) transition. The heat capacity *C* exhibits a discontinuity at the critical temperature of 2.17 K.

Discovered by P. Kapitza and independently by J.F. Allen and A.D. Misener in 1938, superfluidity is a macroscopic quantum phenomenon. When normal liquid helium boils at a temperature above 2.17 K, the boiling stops suddenly as the temperature drops

down to 2.17 K, below which the fluid becomes a superfluid. This sudden transition is reflected in the change of the heat capacity with temperature, as shown in the diagram in **Fig. 2.1**. The liquid-superfluid phase transition manifests itself as a discontinuity of the temperature dependence of heat capacity, which looks like the Greek letter λ (lambda); hence the phase transition was named a *lambda* transition, see **Fig. 2.1**. Below the λ point, liquid helium can flow through a thin capillary (0.5 μm in Kapitza's experiment) frictionlessly, a phenomenon for which Kapitza coined the term superfluidity.

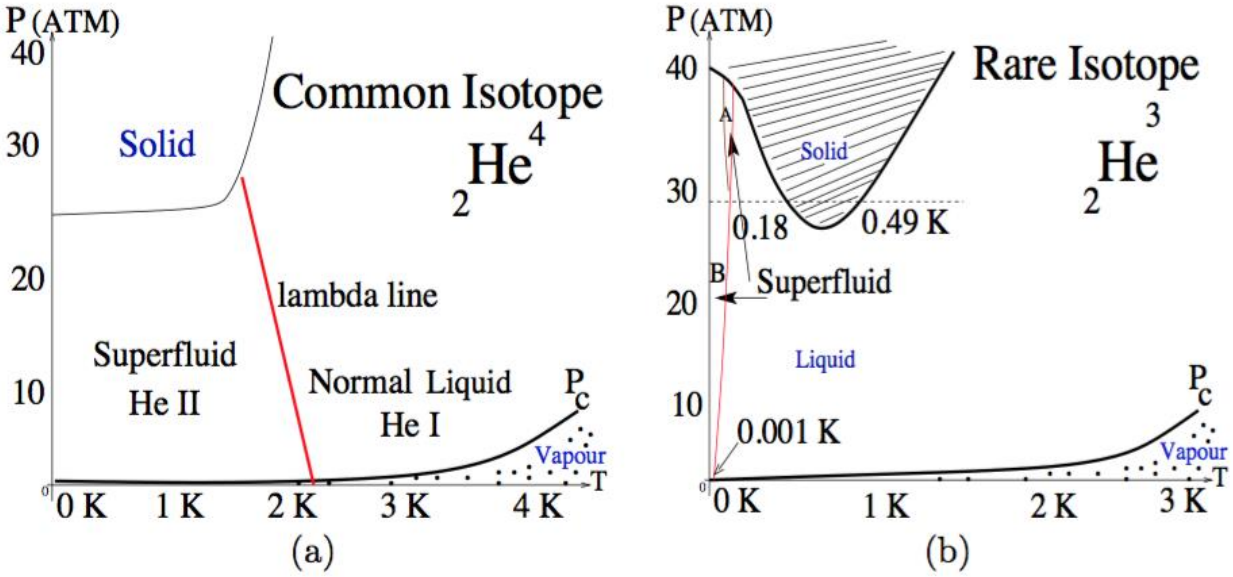

Fig. 2.2. (a) ^{4}He phase diagram. Above 2.17 K, ^{4}He behaves as a liquid, below 2.17 K, ^{4}He behaves as a superfluid, the so-called He II state. **(b)** ^{3}He phase diagram. At high pressure and low temperature, ^{3}He exists in the solid state, whereas at an even lower temperature (lambda point around 1 mK) it enters the superfluid state. [10]

The two stable isotopes of helium obey different quantum statistics: while ^{3}He is a *fermion*, ^{4}He is a *boson*. Note that fermions have a half-integral and bosons an integral spin. This fundamental difference is reflected in their phase diagrams, see **Fig. 2.2**. Each isotope can occur as vapor, liquid, superfluid and solid. However, the pressure and temperature ranges where these phases appear are distinctive. The liquid phase of ^{4}He (also called Helium I) is separated from the superfluid phase (also called Helium II) by the lambda line. Either isotope solidifies at pressures in excess of 25 bars. The superfluidity of ^{4}He arises due to the Bose-Einstein condensation of the ^{4}He atoms into

their quantum ground state. This happens when the (temperature-dependent) de Broglie wavelength exceeds the mean distance between the atoms. Note that ^{3}He cannot form a Bose-Einstein condensate directly, because of its fermionic character: the Pauli exclusion principle then precludes the occupation of the same state by more than one ^{3}He atom. However, the fermionic ^{3}He atoms can form Cooper pairs (like electrons in a superconductor), which are bosonic and thus can undergo Bose-Einstein condensation, however at much lower temperatures, see **Fig. 2.2**.

2.2 Helium Nanodroplet Isolation (HENDI)

Molecular spectroscopy is one of the principle techniques for investigating the structure, properties and interactions of molecules as well as for detecting their presence in the atmosphere and the interstellar space. Due to the complexity of molecules – and the number and variety of their states, molecular spectra are often congested and therefore difficult to assign. For that reason, cooling of the molecules is essential. As in matrix isolation spectroscopy (freezing of molecules in solid rare-gas matrices), in a He-nanodroplet the dopant species is at a thermal equilibrium with the host system. However, the thermodynamically defined ambient temperature of helium nanodroplets is as low as 0.37±0.1 K, which is over an order of magnitude less than the temperatures found in conventional solid rare-gas matrices or standard supersonic jet expansions. The temperature of 0.37 K is reached via evaporative cooling under a high vacuum, a process which is reactivated upon any energy intake by the helium droplet, such as a pick-up of a dopant atom or molecule. Moreover, the superfluid phase, unlike the solid phase of a matrix, affords a nearly-free mobility of the dopant species embedded in the helium droplet. The use of helium nanodroplets as matrices for spectroscopy was pioneered by the groups of P. Toennies [11] and G. Scoles – and termed Helium Nanodroplet Isolation (HENDI).

A typical experimental setup for HENDI spectroscopy is shown in **Figs. 2.3**. The setup consists of two pumped vacuum chambers, namely a source chamber and a detection chamber. The helium droplets are formed in the source chamber via a supersonic expansion of He gas through a small nozzle with a diameter of 5 μm. The source pressure and temperature are set typically to 20 to 100 bar and 20 to 5 K. The supersonic expansion entails adiabatic cooling of helium along the lambda line of the

phase diagram, see **Fig. 2.2.a**. Under vacuum, the droplets cool down further by evaporation to 0.37 K. This uniform terminal temperature is determined by the surface tension of liquid helium. The droplet size varies with the source pressure and temperature and its distribution is log-normal. The droplets are doped with one or more atomic or molecular species by passing the droplet beam through one or more pick up cells (one atom or molecule at a time) and subject to a spectroscopic measurement in the detection chamber. The helium nanodroplet laboratory of Prof. A. Slenczka at the University of Regensburg with which Prof. Friedrich collaborates uses optical spectroscopy: fluorescence of the dopant molecules is excited by a tunable laser at right angles to the droplet beam and collected by a photomultiplier tube. The fluorescence signal can be dispersed. Two electronic states, each hosting vibrational and rotational states, are involved in an optical transition.

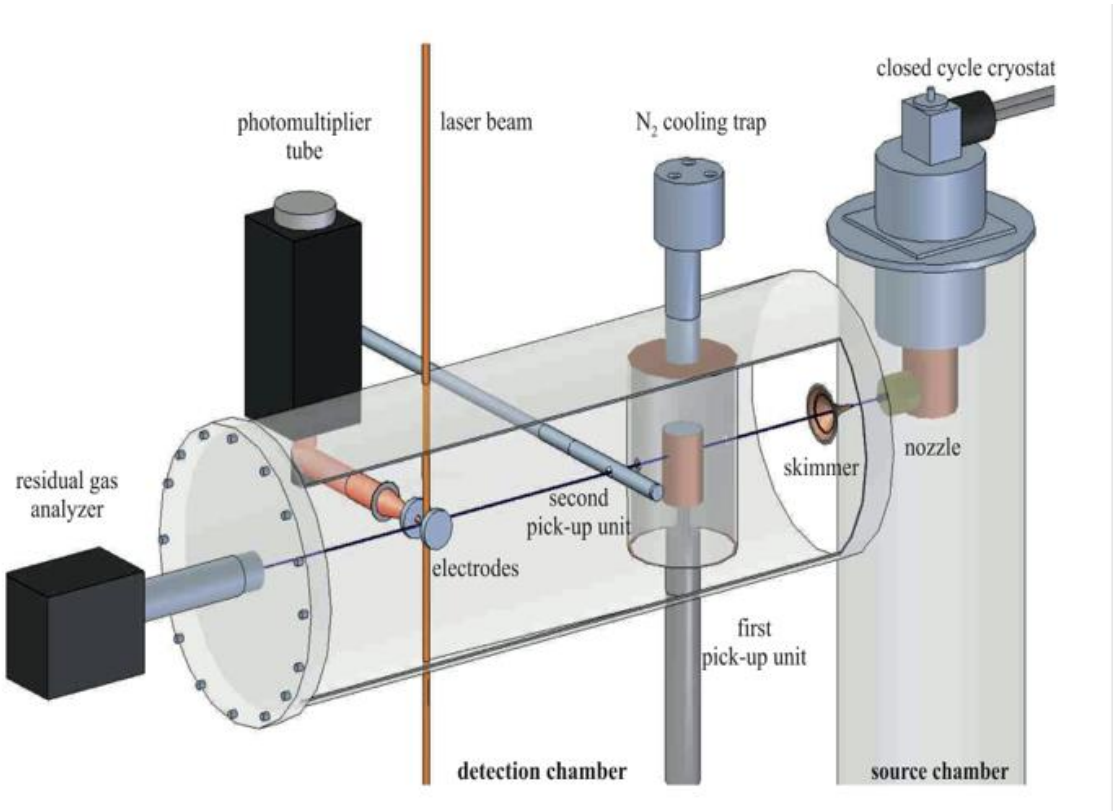

Fig. 2.3. Helium nanodroplet isolation (HENDI) spectroscopy apparatus of the Slenczka group at the University of Regensburg [12].

At a distance of 9 cm downstream from the skimmer the droplet beam passes through the first pick-up cell of a length of 20 mm. The cell is filled with the vapor of a chromophore atom or molecule – the dopant species. The pick-up cell can be heated up to 400 C in order to increase the vapor pressure of species such as metals or large organic molecules. Another 4 cm downstream there is another pick-up cell consisting of a stainless steel pipe 15 cm long. The pick-up process results in a reduction of the initial droplet size due to He-atom evaporation – in response to the energy transfer from the dopant molecule to the droplet. For instance, upon doping an SF_6 molecule into a helium droplet, approximately 600 He atoms are evaporated. [13]

At about 17 cm downstream from the skimmer, the doped He droplet beam is irradiated at right angles by a laser beam and the excited fluorescence detected at right angles to the plane of the two beams by a photomultiplier tube.

The apparatus also enables to carry out the spectroscopic measurement in an electrostatic field (a Stark field): two capacitor plates to which a high-voltage can be applied are mounted parallel to the plane of the two beams and the fluorescence is collected through one of them, see **Fig. 2.3**.

At the rear end of the detection chamber, a residual gas analyzer controls the position of the nozzle and monitors the droplet formation. This analyzer is a quadrupole mass filter (Inficon Transpector H300M) working in the mass-to-charge ratio range of 1-300 amu.

2.3 Line broadening and spectral line-shape

The spectral line that corresponds to a transition between two quantum states 1 and 2 of an atom or molecule is not a delta function, but rather a symmetric or sometimes even asymmetric "peak" centered at the resonance frequency $\nu_0=(E_2-E_1)/h$, with $E_{1,2}$ the energy of states 1 and 2 and h the Planck constant. The width of the spectral line (*line width*) and shape (*line shape*) is determined by a convolution of various broadening mechanisms. The first and foremost such mechanism is the *natural* broadening that arises due to the finite width of the energy levels themselves – as dictated by the uncertainty principle: the shorter the lifetime of a given level, Δt, the wider its energy spread, ΔE, i.e., $\Delta E\, \Delta t \approx h$. Note that only the ground level is sharp, with an infinite lifetime. The shape of a naturally broadened line is a *Lorentzian*,

$$L(x) = (1+x^2)^{-1} \quad \text{with} \quad x=2(\nu_0-\nu)/\Delta\nu \qquad (1)$$

where $\Delta\nu$ is the full width at half maximum, see **Fig. 2.4**. Natural broadening is homogeneous, in the sense that the line shape of all atoms or molecules for a given transition is given by the same Lorentzian.

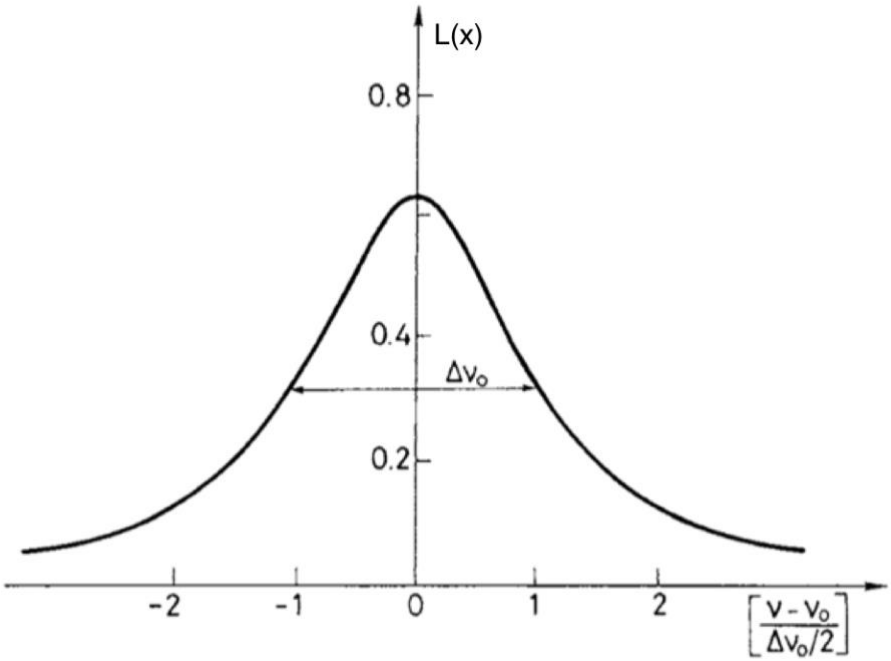

Fig. 2.4 The Lorentzian function

The Maxwell-Boltzmann distribution of the molecular velocities translates into a *Gaussian* line shape of a given spectral line,

$$G(x)= \exp [-(\ln 2)x^2] \qquad (2)$$

see **Fig. 2.5**. Note that both the Lorentzian and the Gaussian are centered at ν_0 and have the value 1 at the maximum and ½ at the full width at half maximum. The line broadening due to the velocity distribution is inhomogeneous, as it is different for different molecules in a given sample, depending on their state of motion.

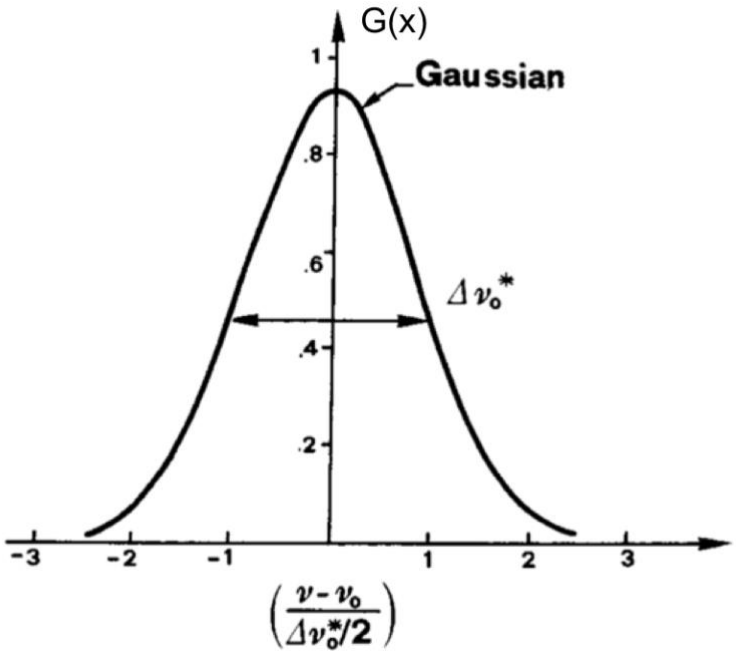

Fig. 2.5 Plot of Gaussian function

In He droplets, an additional type of inhomogeneous broadening is at play that arises from the convolution of the nascent droplet size distribution *p(N)* (the size of a droplet is given by the number N of He atoms it is comprised of) and by the probability distribution *q(k,N)* that a droplet of size N will pick up k molecules on flight through the pick up cell. At the end, the droplet consists of N-ΔN helium atoms as ΔN atoms evaporated in the process of dissipating the energy of the picked up species. The inhomogeneous distribution function is then given by [14]

$$G^*(\nu') = \int dN p(N)\, q(k,N)\, \delta(\nu' - \nu(k, N-\Delta N)) \qquad (3)$$

For OCS as an example, for N = 1000, the spectral line of OCS is broadened to about 300 MHz. However, for N = 6000, the line width of OCS decreases to about 150 MHz.

We note that whereas small molecules (with large rotational constants) have been observed to relax by exciting the bulk modes of the droplet, large molecules (with small rotational constants) relax either by rotation-translation energy transfer or by coupling to the surface modes of the droplet. While the former process leads to homogeneous broadening, the latter contributes to inhomogeneous broadening of the spectral lines.

In summary, the factors determining inhomogeneous broadening are the droplet size distribution, the pickup probability, and the droplet size-dependent center frequency. On

the other hand, the dynamics of the rotational relaxation in the droplet contributes to the homogeneous broadening.

2.4 Interaction between the dopant and the helium environment

A classical theory assumes that the helium solvent forms *a non-superfluid shell* around the dopant molecule. [15-22] Due to its high density (average distance of 4 Å) and strong interaction, such a solvation shell rotates together with the molecule, thereby increasing its effective moment of inertia – and reducing its rotational constant. [3,5,23].

Recently, Mikhail Lemeshko presented a novel quantum approach to treating the dopant-He droplet interaction, which is based on a quasi-particle termed the angulon (a quantum rotor dressed in the field of the bulk phonons of the helium environment). The angulon interaction is described by a Hamiltonian consisting of three terms: The first term represents the rotational kinetic energy of the rotor. The second term describes the bosonic bath. And the third term the coupling between the dopant and the helium bath. The strength of this interaction is characterized by a dimensionless parameter

$$\gamma = \frac{B}{\Delta} \qquad (4)$$

The parameter γ is inversely proportional to the anisotropy parameter Δ of the molecule interacting with the helium bath. For $\gamma < 1$, the coupling between the dopant and the helium bath is strong, for $\gamma > 1$ it is weak.

2.5 Stark spectroscopy as a means to distinguish isomeric variants of species embedded in He nanodroplets

The observation of more than a single electronic origin from resonances assigned to an identical stoichiometry (a monomer, a dimer, etc.) of the species embedded in He droplets reveals the presence of isomeric variants. As the isomeric variants arise from the intermolecular dispersion interaction within the complex, their identification provides a valuable insight into binding by dispersion forces. In fact, the elucidation of London dispersion forces via the study of molecular complexes created and probed in

He droplets is the subject of the DFG-funded joint project between the research groups of Profs. Friedrich (Berlin) and Slenczka (Regensburg) that provided the environment for my BA thesis.

The ultimate step in the analysis of van der Waals complexes which goes beyond the identification of the number of isomeric variants is the analysis of the intrinsic configuration of each complex. The configuration correlates with the mass distribution which, in turn, determines the moments of inertia of the complex. Thus, the measurement of the moments of inertia provides an insight into the configuration of the complex. Apart from rotationally resolved field-free spectra, the moments of inertia can be also obtained with high sensitivity via Stark spectroscopy [24–26], where a static electric field generates a cosine potential for a dipolar dopant. Since the Stark shift is proportional to the moment of inertia and the molecular electric dipole moment – both of which are key structural indicators – Stark spectroscopy is the method of choice for studying complex species embedded in He droplets.

3. Method

Our chief method is to simulate the rotational spectra of molecules, actual or model, using PGOPHER (version 10.0.505). Both field-free and Stark spectra with varying sets of rotational constants are simulated.

Table 1 lists the molecular constants used as simulation parameters.

Molecules	Gas-phase			Helium environment			References
	B"	B'	v_0	B"	B'	v_0	
HCCCN	0.15162	0.15134	3327.37	0.05249	0.05189	3327.09	[27] [28]
$OC^{32}S$	0.20286	0.20164	2062.20	0.07442	0.0732	2061.64	[29]
HCN	1.47822	1.4680	2096.84	1.2045	1.175	3311.20	[30]
HF	20.56	19.79	3961.42	20.2518	19.48	3959.19	[31] [32]
NH_3	10.07	9.95	932.43	7.65	7.5	949.83	[33]
CH_3CCH	0.285	0.284	3335.06	0.0741	0.073	3334.90	[34]
Glyoxal	0.160	0.154	21973.50	0.0722	0.055	21942.18	[35]
I_2	0.0373	0.0372	15724.57	0.0224	0.0223	15728.35	[36][37][38]
SF_6	0.09108	0.09108	948.102	0.03396	0.03396	946.562	[39]
CS_2	0.109	0.108	1535.356	0.111	0.110	1535.532	[40] [41]
CO_2	0.3902	0.3875	3612.837	0.156	0.154	3612.420	[42]
N_2O	0.4242	0.4190	3480.819	0.0742	0.0717	3482.00	[42]
NO	1.720	1.672	1876.08	1.307	1.253	1875.65	[27] [43]
CO	1.919	1.910	2143.27	0.2895	0.2893	2143.24	[44] [45]
HCl	10.44	10.13	2885.98	0.310	0.305	2907.08	[46][47][48]
CH_4	5.256	5.196	3019.52	5.01	4.93	3020.32	[49]

Table 1. Rotational constants and band origin in gas-phase and helium environment respectively, for some simple molecules

3.1 PGOPHER: A program for simulating and fitting rotational, vibrational, and electronic spectra

The general purpose of the PGOPHER program is simulating and fitting rotational, vibrational and electronic molecular spectra. [8] Since the calculation makes no difference between the vibrational and electronic components of wavefunction, this program uses generally the main concept of vibronic state, in which the information about symmetry, the energy in the absence of rotational motion (band origin) and at least one rotational constant for each vibronic state are minimally already provided.

The calculation is organized by means of a series of object described in the tree structure shown in **Fig. 3.1.**

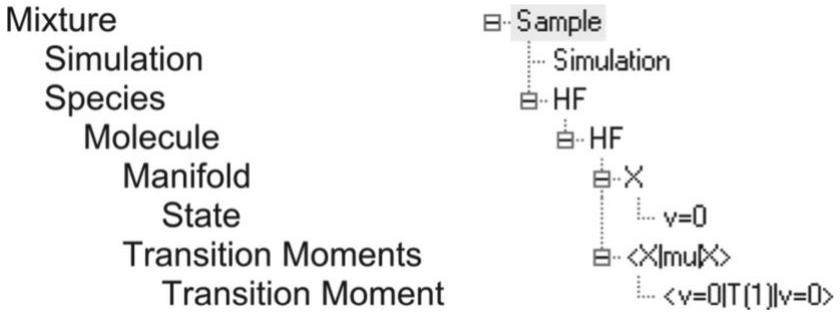

Fig. 3.1 Tree structure organization of a typical simulation in PGOPHER [8]

The object *State* plays the role of key organizer in the calculation containing the information about symmetry, band origin and the rotational constants for a single vibronic state. This object can consist of more than one states grouped under the object *Manifold*, which is virtually specified as the electronic states classified in the object *Molecule*. The possible transitions between vibronic states connecting the manifolds are set up in the object *Transition Moment* grouped under the object *Transition Moments* containing the transition dipole moment of each transition. In the presence of external electric or magnetic field, the object *Simulation* can be set up by entering the electric field or magnetic field magnitude. In the default mode, the program assumes the light to be unpolarized. Hence, a new object called *Polarisation* need to be created under the object *Simulation* to specify if the light is parallel or perpendicular polarized.

The wavefunction for a given rovibronic state Ψ_i, is expanded as a linear combination of basis states $|j>$: [8]

$$\Psi_i = \sum_j c_j^i |j> \quad (5)$$

The coefficients vector c_j, is obtained by diagonalizing the Hamiltonian matrix that has been set up in an appropriate basis set. The fundamental basis state is described in the form $|\eta sJKM>$, where η describes rovibronic state in state object and also the total electronic spin, *s* describes the symmetry of the state, *J* describes the total angular momentum, K describes the projection of J along the molecule-fixed axis, and *M* describes the projection along the laboratory axis. The quantum number *M* is not required in the absence of external electric or magnetic field (field free case). The diagonalized Hamiltonian matrix results in a set of eigenvalues that represent the molecular energy levels. These energy levels are specified according the eigenvalue numbers *i* in the sequence of increasing energy levels.

Making a data file in PGOPHER is initiated by choosing **File >> New >> "Molecule Type" (Linear Molecule/Symmetric Top/Asymmetric Top).** It is important, that the program can identify the type of molecule, since every type of molecule has its specific unit in this program, which can affect the rotational structure of certain vibronic state. To set up the data file will be outlined according to molecule type below. For the case of molecule type *spherical top*, the data file will be set up to an approximation of molecule type *symmetric top*, by treating the parameter B and C in symmetric top-setting equally, since projected rotational constants A, B, C along molecular axis in spherical top are equally same.

3.1.1 Linear molecules

The rotational Hamiltonian is described by

$$\hat{H}_{rot} = B_v \hat{\boldsymbol{R}}^2 = B_v(\hat{\boldsymbol{N}} - \hat{\boldsymbol{L}})^2 = B_v((\hat{\boldsymbol{J}} - \hat{\boldsymbol{S}}) - \hat{\boldsymbol{L}})^2 = B_v(\hat{\boldsymbol{J}} - (\hat{\boldsymbol{L}} + \hat{\boldsymbol{S}}))^2 \quad (6)$$

The angular momentum operators appear in bold, where **R** is the rotational angular momentum of the bare nuclei, **N** is the total angular momentum excluding electron spin, **L** is the orbital angular momentum, **J** is the total angular momentum excluding nuclear spin, and **S** is the angular momentum of electronic spin. Certain special ways of coupling of these angular momenta result in the so-called Hund's coupling cases that apply exactly or approximately to a wide variety of real molecules.

For calculating the linear molecules, a Hund's case (a) is used basically, in order to have basis sates $|\eta\Lambda S\Sigma J\Omega M\rangle$, hence 2S+1 fine structure states can have relative energies BJ(J+1) characterized by $\boldsymbol{\Omega}$. This omega parameter $\boldsymbol{\Omega}$ defines angular momentum vector along the internuclear axis as the sum of $\boldsymbol{\Omega} = \boldsymbol{\Lambda}+\boldsymbol{\Sigma}$, the projection of L and S respectively. It is valuable for molecular state having $\Lambda \neq 0$, $\Sigma \neq 0$. If the rotational Hamiltonian (7) is diagonalized in Hund's case (a) basis state, we can obtain

$$\langle \mathbf{J\Omega M} \mid \hat{H}_{rot} \mid \mathbf{J\Omega M} \rangle \qquad (7)$$

$$= \langle \mathbf{J\Omega M} \mid B_v(|\boldsymbol{J}|^2 - |\boldsymbol{\Omega}|^2) + A\boldsymbol{\Lambda}\cdot\boldsymbol{\Sigma} \mid \mathbf{J\Omega M} \rangle \qquad (8)$$

$$E_{rot} = B_v\,(J(J+1) - \Omega^2) = A\Lambda\Sigma \qquad (9)$$

A is the molecular spin-orbit coupling constant of molecular state $\Lambda \neq 0$ of certain molecules. Molecular ground state has no spin-orbit coupling constant, because the projection of orbital angular momentum Λ has zero value, except for certain molecules such as Nitric Oxide, whose molecular ground state possess *pi* Π-State. [27]

In case of presence of external electric field, omega parameter Ω can be picked as a criterion of choosing the *Jmax* Parameter in Object *Species*. This can help in calculation, since a calculation in case of presence of external field can takes much more time than in case of absence of external field. Even it does not rule out a possibility, that the used device will be damaged.

Making a linear molecule data file in PGOPHER is initiated by choosing **File >> New >> Linear Molecule.** The parameter needed to set up in making linear molecule data file will be spelled out through following **Table 1**.

Object	Parameter	Details
Simulation	Temperature	Rotational temperature in Kelvin
	Gaussian	Gaussian contribution to Full Width Half Maximum (FWHM)
	Lorentzian	Lorentzian contribution to Full Width Half Maximum (FWHM)
Species	Jmin	Minimum J to use in calculation
	Jmax	Maximum J to use in calculation
	Efield	Static electric field in V/m, in case of Stark Spectroscopy
Molecule	Symmetric	If the molecule has centre of symmetry, this setting is *true*
State	Origin	Band origin of the state

	B	Rotational constant
	A	Spin-orbit coupling constant, if the state possesses $\Lambda \neq 0$, $\Sigma \neq 0$
	S	The electron spin
	Lambda	Body-fixed Z-axis component of the orbital angular momentum quantum number, L
	gerade	If the symmetric setting is *true* and it is gerade *g*, this setting is *true*, if it is ungerade *u*, this setting is false. But if the symmetric setting is already *false*, this setting can be ignored in its default setting
Transition moment	Strength	The transition dipole moment of corresponding states transition, in Debye. In case of presence of external field, it is needed to create transition moments <*Ground*|*mu*|*Ground*> and <*Excited*|*mu*|*Excited*> and set the strength of transition dipole moment of each transition moment. The strength of transition moment <*Ground*|*mu*|*Excited*> can be neglected as 1.

Table 2. A list of parameters for a typical PGOPHER simulation of a linear molecule

3.1.2 Symmetric tops

For symmetric top molecules, the rotational Hamiltonian is described by the following equation

$$\begin{aligned}\hat{H}_{rot} = B\,\hat{\mathbf{N}}^2 + (C-B)\hat{\mathbf{N}}_z^2 + (-2C\zeta + \eta_J\hat{\mathbf{N}}^2 + \eta_K\hat{\mathbf{N}}_z^2 +)\,\hat{\mathbf{l}}_z\hat{\mathbf{N}}_z \\ - D_J\hat{\mathbf{N}}^4 - D_{JK}\hat{\mathbf{N}}^2\hat{\mathbf{N}}_z^2 + - D_K\hat{\mathbf{N}}_z^4 \\ + H_J\,\hat{\mathbf{N}}^6 + H_{JK}\,\hat{\mathbf{N}}^4\hat{\mathbf{N}}_z^2 + H_{KJ}\,\hat{\mathbf{N}}^2\hat{\mathbf{N}}_z^4 + H_K\hat{\mathbf{N}}_z^6 \\ + L_J\hat{\mathbf{N}}^8 + L_{JJK}\,\hat{\mathbf{N}}^6\hat{\mathbf{N}}_z^2 + L_{JK}\,\hat{\mathbf{N}}^2\hat{\mathbf{N}}_z^4 + L_{KKJ}\hat{\mathbf{N}}^2\hat{\mathbf{N}}_z^6 + L_K\hat{\mathbf{N}}_z^8 \qquad (10)\end{aligned}$$

Calculating in case of symmetric top molecules uses the basis states $|\eta JNK\boldsymbol{l}\rangle$, where **K** is the projection of N on to the highest order symmetry axis and $\boldsymbol{l}$ is the label of the vibronic component. If the rotational Hamiltonian (10) is diagonalized in this basis state, we can obtain

$$\begin{aligned}E_{rot} = \nu_0 \\ + B\,N(N+1) + (C-B)K^2 + (-2C\zeta + \eta_J N(N+1) + \eta_K K^2)\,lK \\ - D_J N^2(N+1)^2 - D_{JK}N(N+1)K^2 - D_K K^4\end{aligned}$$

$$+ H_J N^3(N+1)^3 + H_{JK} N^2(N+1)^2 K^2 + H_{KJ} N(N+1) K^4 + H_K K^6$$
$$+ L_J N^4(N+1)^4 + L_{JJK} N^3(N+1)^3 K^2 + L_{JK} N^2(N+1)^2 K^4 + L_{KKJ} N(N+1) K^6 + L_K K^8$$
$$+ \tfrac{1}{2}\varepsilon_{bb}(N_+ S_- + N_- S_+) + \varepsilon_{cc} N_z S_z + D^s_N \mathrm{N}^2\mathrm{N.S} + \tfrac{1}{2} D^s_{NK}(\mathrm{N}^2 N_z S_z + N_z S_z \mathrm{N}^2) + D^s_{KN} \mathrm{N.S} N_z^2$$
$$+ \alpha(3S_z^2 - \mathrm{S}^2) + \tfrac{1}{2}\beta(S_+^2 + S_-^2) + a_{\mathrm{eff}} l S_z \qquad (11)$$

ζ (*zeta*) is a the Coriolis coupling constant, which is essential, if the vibronic state is a degenerate state such as E symmetry-state.

Making a symmetric top molecule data file in PGOPHER is initiated by choosing **File >> New >> Symmetric Top.** The parameter needed to set up in making linear molecule data file will be spelled out through following **Table 2**

Object	Parameter	Details
Simulation	Temperature	Rotational temperature in Kelvin
	Gaussian	Gaussian contribution to Full Width Half Maximum (FWHM)
	Lorentzian	Lorentzian contribution to Full Width Half Maximum (FWHM)
Species	Jmin	Minimum J to use in calculation
	Jmax	Maximum J to use in calculation
	Efield	Static electric field in V/m, in case of Stark Spectroscopy
Molecule	Point Group	Point group of molecule
State	Origin	Band origin of the state
	A/C and B	Rotational constant
	Zeta	Coriolis coupling constant, for degenerate (E Symmetry) vibronic state
	S	The electron spin
	Symmetry	The particular symmetry of the state
Transition moment	Strength	The transition dipole moment of corresponding states transition, in Debye. In case of presence of external field, it is needed to create transition moments <*Ground*|*mu*|*Ground*> and <*Excited*|*mu*|*Excited*> and set the strength of transition dipole moment of each transition moment. The strength of transition moment <*Ground*|*mu*|*Excited*> can be neglected as 1.

Table 3. A list of parameters for a typical PGOPHER simulation of a symmetric top

For case of molecule type spherical top, the parameter A/B and C will be equally treated, since rotational constants A, B, C along molecular axis in spherical top are equally same.

3.1.3 Asymmetric tops

Compared to other molecule type, the case of asymmetric top should be treated particularly, since all the principal inertial axis possess different moment of inertia $I_a \neq I_b \neq I_c$. Therefore, it's important in choosing the axis used to define *K*, since this quantum number is here quantized in molecule fixed *z*-axis, but this can be pictured either in principal inertia axis *a, b,* or *c*. Once the choice for *z*-axis has been decided, we must also decide which principal axis is suitable for molecule fixed *x*- and *y*-axis.

To facilitate this work, there are six possible choices giving a representation of molecule fixed *x, y, z* axis to the principal inertia axis *a, b, c*. This representation must be included in the setting of making data file of asymmetric top molecule, since the parameters in this program are specified in terms of operators in the molecule fixed axis, not in the principal inertial axis applied to define the rotational constants A, B, and C. The representation is presented in **Table 3** below.

	Representation					
	I*r*	II*r*	III*r*	I*l*	II*l*	III*l*
z	a	b	c	a	b	c
x	b	c	a	c	a	b
y	c	a	b	b	c	a

Table 4. Various representations for an asymmetric top mixture

Calculating in the case of asymmetric top molecules uses the basis state of symmetric top case without involving the quantum number *l*, so **|ηJNK>.** The Hamiltonian in this case is stated into two forms, namely *standard* form

$$\hat{H}_{rot} = A\hat{J}_a^2 + B\hat{J}_b^2 + C\hat{J}_c^2 \quad (12)$$

and alternate form

$$\hat{H}_{alt} = A\hat{J}_z^2 + B(\hat{\boldsymbol{J}}^2 - \hat{J}_z^2) + 1/4\delta\,(\hat{J}_+^2 + \hat{J}_-^2) \qquad (13)$$

For case of asymmetric top molecules having similar two rotational constants, such as near-prolate top molecule B ≈ C, the alternate form can give an exact calculation.

Making am asymmetric top molecule data file in PGOPHER is initiated by choosing **File >> New >> Asymmetric Top.** The parameter needed to set up in making linear molecule data file will be spelled out through following **Table 4**

Object	Parameter	Details
Simulation	Temperature	Rotational temperature in Kelvin
	Gaussian	Gaussian contribution to Full Width Half Maximum (FWHM)
	Lorentzian	Lorentzian contribution to Full Width Half Maximum (FWHM)
Species	Jmin	Minimum J to use in calculation
	Jmax	Maximum J to use in calculation
	Efield	Static electric field in V/m, in case of Stark Spectroscopy
Molecule	Point Group	Point group of molecule
	Representation	See **Table 4**
	eeWt	Statictical weight for *ee* levels for totally symmetric vibronic states
	eoWt	Statictical weight for *eo* levels for totally symmetric vibronic states
	oeWt	Statictical weight for *oe* levels for totally symmetric vibronic states
	ooWt	Statictical weight for *oo* levels for totally symmetric vibronic states
State	Origin	Band origin of the state
	A, B and C	Rotational constant A, B, and C
	S	The electron spin
	Symmetry	The particular symmetry of the state
Transition moment	Axis	The axis of transition dipole moment for **Cartesian transition moment**
	Strength	The transition dipole moment for **Spherical transition**

		moment, (in Debye). In case of presence of external field, it is needed to create transition moments <*Ground*|*mu*|*Ground*> and <*Excited*|*mu*|*Excited*> and set the strength of transition dipole moment of each transition moment. The strength of transition moment <*Ground*|*mu*|*Excited*> can be neglected as 1.

Table 5. A list of parameters for a typical PGOPHER simulation of an asymmetric top

3.2 Spectral-width analysis

We define the spectral width of a rotational spectrum as the full-width at half maximum (FWHM) of the spectrum convoluted by a Gaussian function of an appropriate width. The width of the convoluting Gaussian must not be too large as to mask all the features of the spectrum, nor must it be too small as to result in too many individual peaks. The spectral width of an effective dopant-He complex rotor relative to that of the dopant alone in gas-phase is defined as the ratio of their FWHMs after convolution by a Gaussian of the same width.

Before studying actual molecules, we simulated some model cases as described in sections 4.2 and 4.3 - the objective being, to identify a dependence, if any, between the relative spectral width and the renormalized rotational constant ratio. The rotational energy for each of the test cases was the same, such that the maximum value of J (the rank at which the Hamiltonian matrix is truncated) supplied to PGOPHER varies in each case, due to varying rotational constants.

4. Results

4.1 Verification of Stark and field-free spectra by comparison with existing literature

We simulated various molecules of linear molecules, symmetric top, and asymmetric top and compared them with the peaks in experimental spectra from literature.

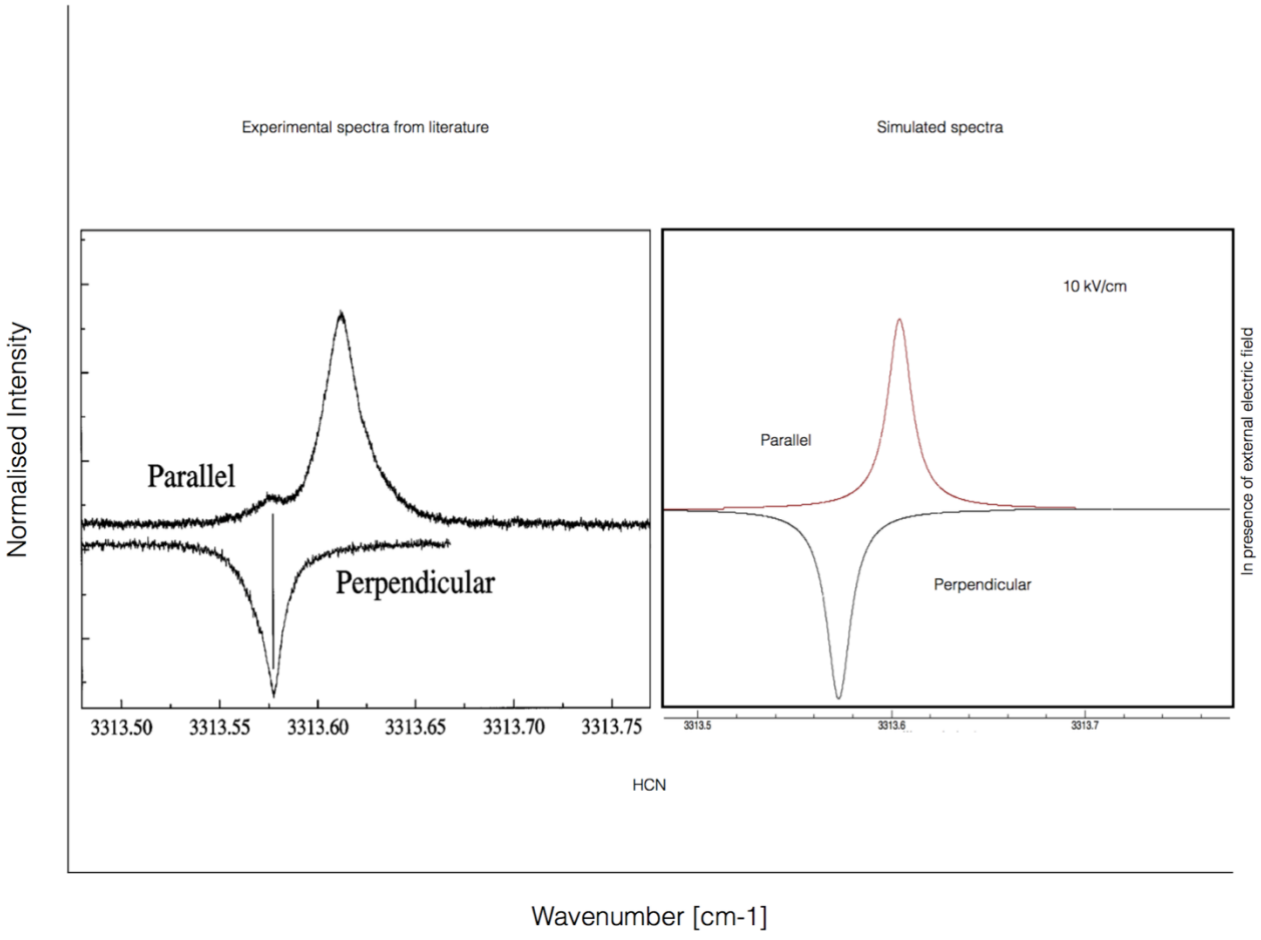

Fig. 4.1 Simulation Stark spectra of HCN molecule. The right column shows a spectra simulated as part of this thesis c.f. experimental spectra shown in the left column. [30] The laser pulse is polarized parallel (top) and perpendicular (bottom) to the applied electric field.

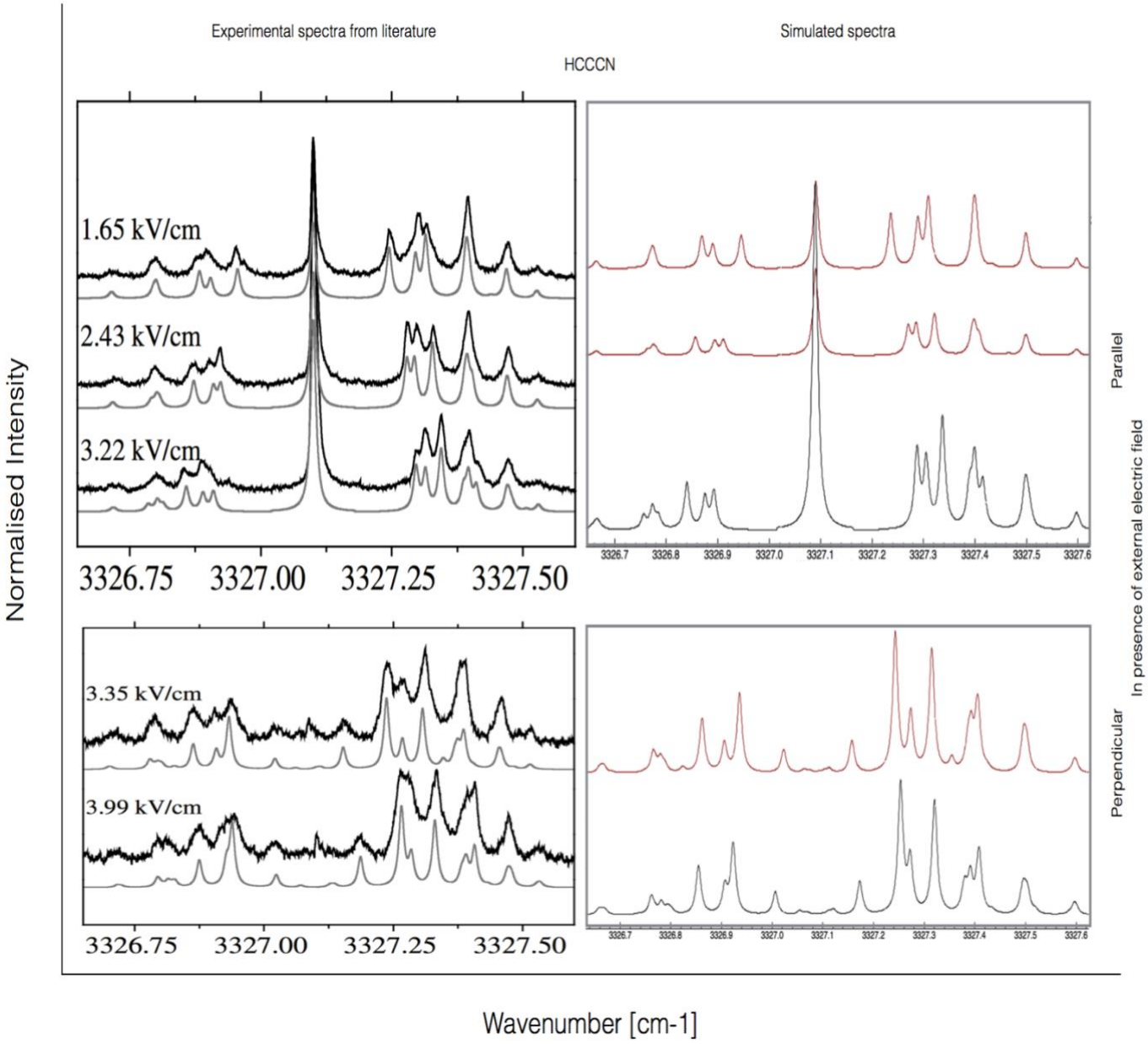

Fig. 4.2 Simulation Stark spectra of HCCCN molecule. The right column shows a spectra simulated as part of this thesis c.f. experimental spectra shown in the left column. [28] The laser pulse is polarized parallel (top) and perpendicular (bottom) to the applied electric field.

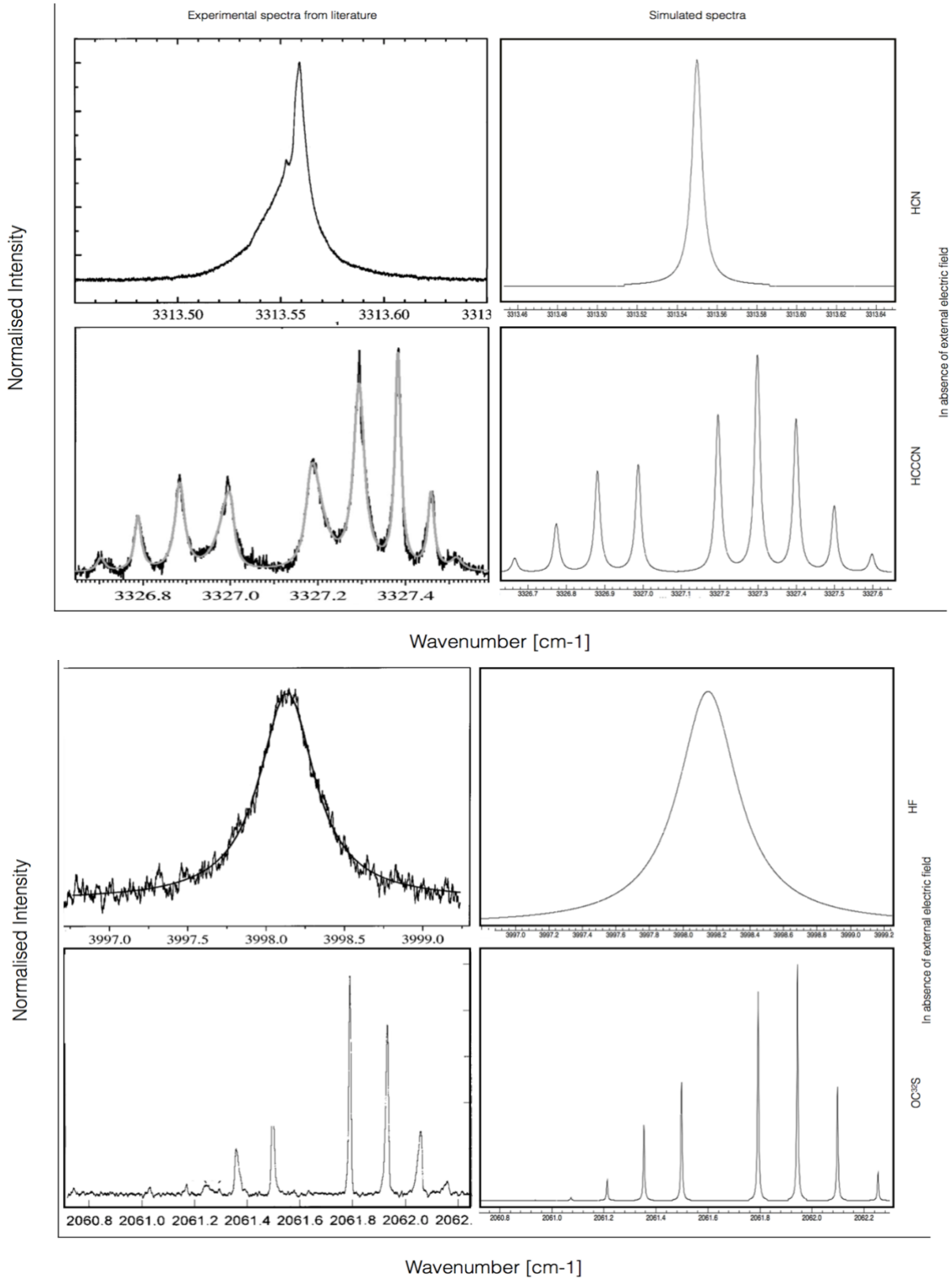

Fig. 4.3 Comparison of simulated field free spectra of some linear rotor molecules with experimental spectra from literature in left column. [28][29][30[32] The figures in right column shows spectra simulated as part of this thesis.

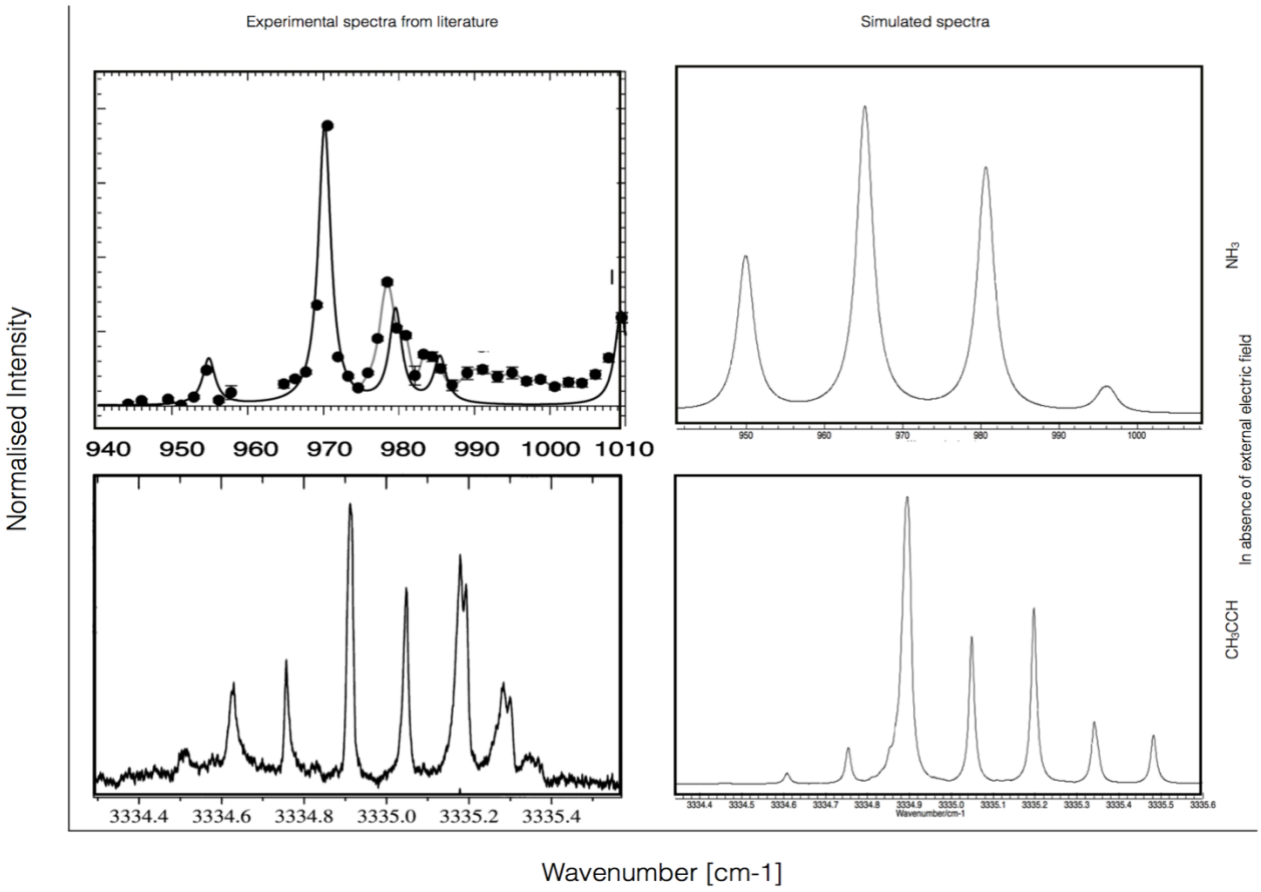

Fig. 4.4 Comparison of simulated field free spectra of some symmetric top molecules with experimental spectra from literature in left column. [33][34] The figures in right column shows spectra simulated as part of this thesis.

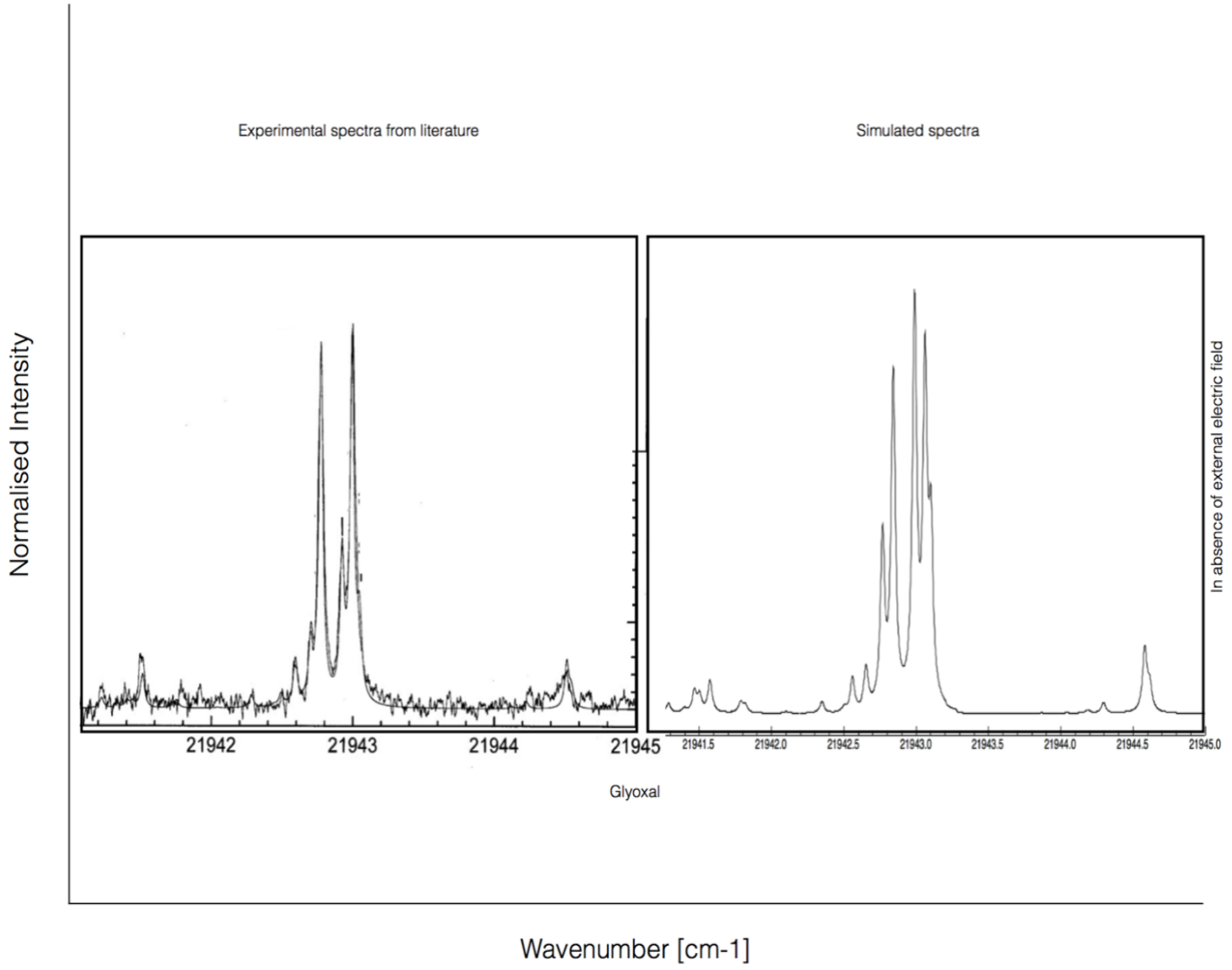

Fig. 4.5 Comparison of simulated field free spectra of asymmetric top molecule with experimental spectra from literature in left column. [35] The figures in right column shows spectra simulated as part of this thesis.

The simulated spectra are compared with the experimental spectra from literature informed in **Table 1.** From all shown figures, we verified some simulated spectra from literatures and we take conclusion that the program PGOPHER works

4.2 Analysis of spectral widths of field-free linear rotors

We consider three model linear rotors in the gas-phase whose rotational constants are separated by an order of magnitude each - 0.001 cm^{-1}, 0.01 cm^{-1} and 0.001 cm^{-1}.

By progressively reducing the rotational constants of each of these, we simulate a possible helium environment effective rotational behavior and calculate the relative spectral-widths from the rotational spectra. **Fig. 4.6a** and **4.6b** show the stick spectra, while the relative spectral-width scaling is plotted in **Fig. 4.8a**. All simulations were performed at 0.37 K.

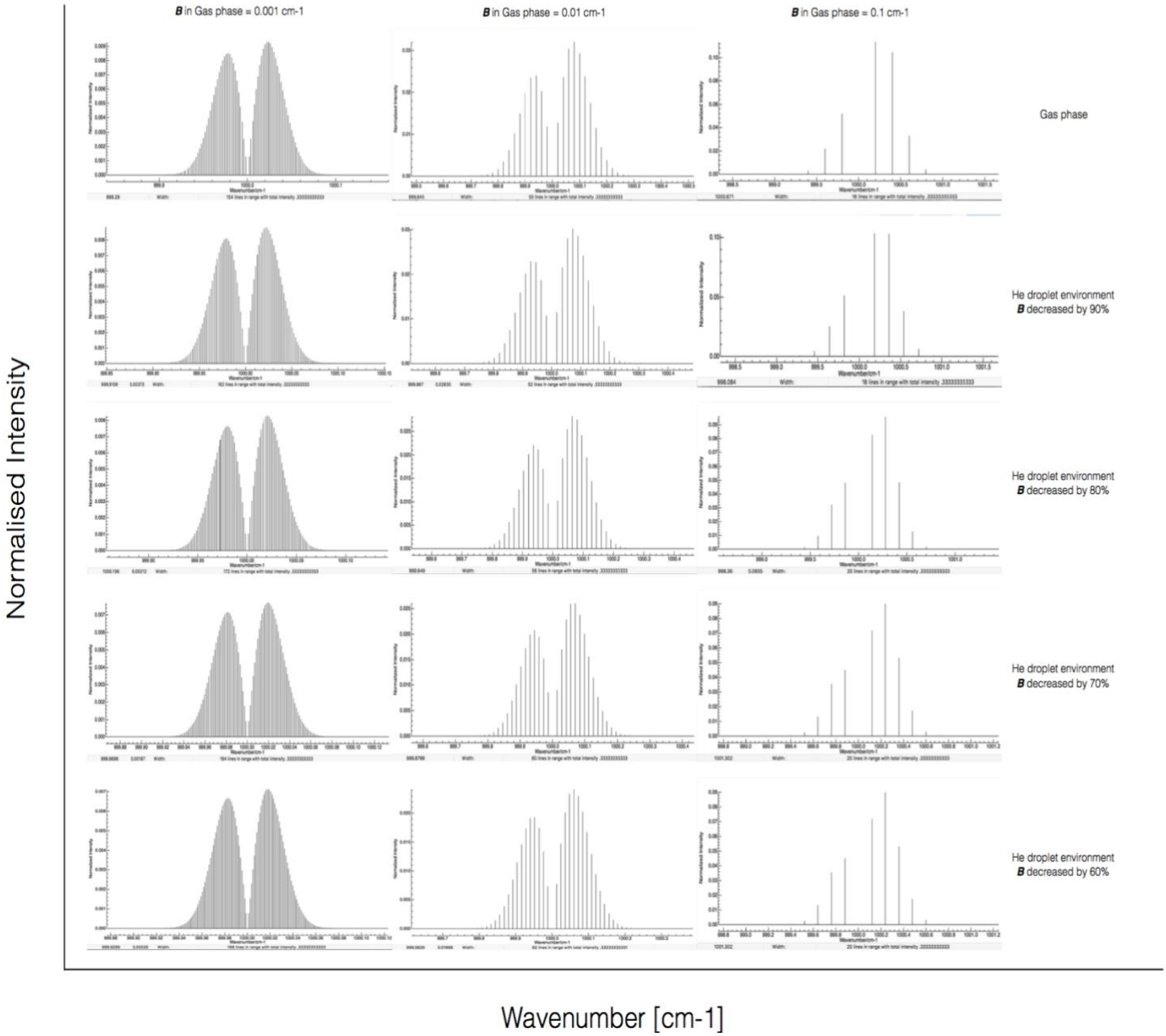

Fig. 4.6a Simulated spectra of field-free model linear rotors with gas-phase rotational constant values 0.001 cm-1, 0.01 cm-1, and 0.1 cm-1, assuming that the rotational constants in helium environment are reduced 60-90% from their gas phase values

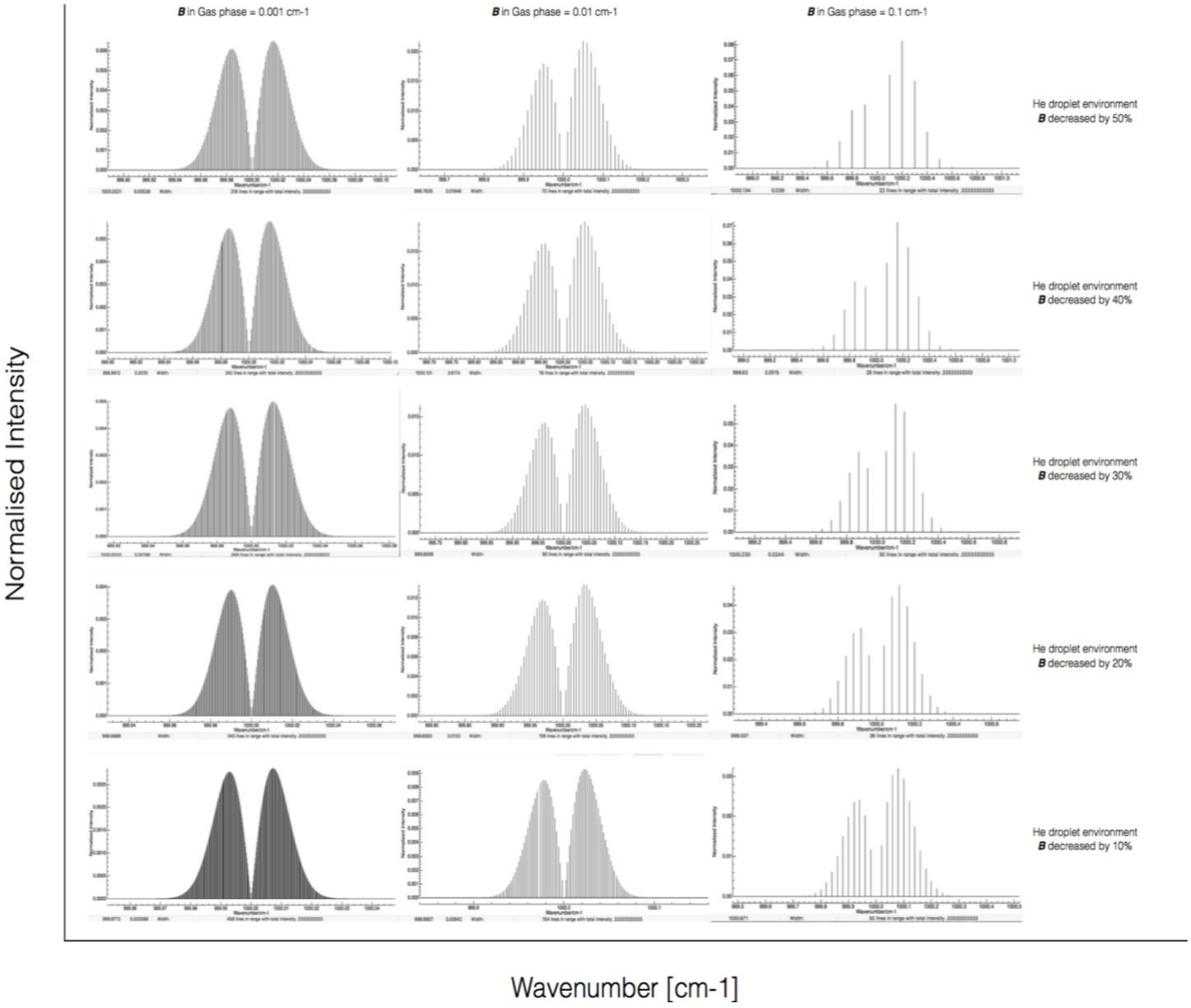

Fig. 4.6b Simulated spectra of field-free model linear rotors with gas-phase rotational constant values 0.001 cm-1, 0.01 cm-1, and 0.1 cm-1, assuming that the rotational constants in helium environment are reduced 10-50% from their gas phase values

Gas phase			Helium			$\frac{FWHM_{He}}{FWHM_{Gas}}$	$\frac{B_{He}}{B_{Gas}}$
B	J-max	FWHM	B	J-max	FWHM		
0.001	77	0.090435	0.0009	81	0.087340	0,965776	0.9
0.001	77	0.090435	0.0008	86	0.083106	0,918958	0.8
0.001	77	0.090435	0.0007	92	0.078574	0.868845	0.7
0.001	77	0.090435	0.0006	99	0.073726	0.815237	0.6
0.001	77	0.090435	0.0005	108	0.068488	0.757317	0.5
0.001	77	0.090435	0.0004	121	0.062519	0.691314	0.4
0.001	77	0.090435	0.0003	134	0.056074	0.620047	0.3
0.001	77	0.090435	0.0002	170	0.047858	0.529198	0.2
0.001	77	0.090435	0.0001	229	0.035198	0.389207	0.1
0.01	25	0.25368	0.009	26	0.24676	0.972722	0.9
0.01	25	0.25368	0.008	28	0.23681	0.933498	0.8
0.01	25	0.25368	0.007	30	0.22205	0.875315	0.7
0.01	25	0.25368	0.006	32	0.20582	0.811337	0.6
0.01	25	0.25368	0.005	35	0.19010	0.749369	0.5
0.01	25	0.25368	0.004	39	0.17027	0.671199	0.4
0.01	25	0.25368	0.003	45	0.14982	0.590586	0.3
0.01	25	0.25368	0.002	53	0.12444	0.490539	0.2
0.01	25	0.25368	0.001	77	0.09135	0.360099	0.1
0.1	8	0.72703	0.09	9	0.74961	1.03106	0.9
0.1	8	0.72703	0.08	9	0.76651	1.05430	0.8
0.1	8	0.72703	0.07	10	0.77015	1.05931	0.7
0.1	8	0.72703	0.06	10	0.76094	1.04664	0.6
0.1	8	0.72703	0.05	11	0.74009	1.01796	0.5
0.1	8	0.72703	0.04	13	0.70815	0.97403	0.4
0.1	8	0.72703	0.03	15	0.66466	0.91421	0.3
0.1	8	0.72703	0.02	18	0.61384	0.84431	0.2
0.1	8	0.72703	0.01	25	0.55744	0.76673	0.1

Table 6. Rotational constants in gas phase of linear rotor and their reduction in helium environment with the corresponding J_{max}

4.3 Analysis of spectral widths of field free symmetric top rotors

We consider three model symmetric top rotors in the gas-phase whose rotational constants *B* are separated by an order of magnitude each - 0.001 cm^{-1}, 0.01 cm^{-1} and 0.001 cm^{-1} and the rotational constant *C* is taken to be half of rotational constant *B*

By progressively reducing the rotational constants *B* of each of these, we simulate a possible helium environment effective rotational behavior and calculate the relative spectral-widths from the rotational spectra. **Figures 4.7a** and **4.7b** illustrate the stick spectra, while the relative spectral-width scaling is plotted in **Figure 4.8a**. All simulations were performed at 0.37 K.

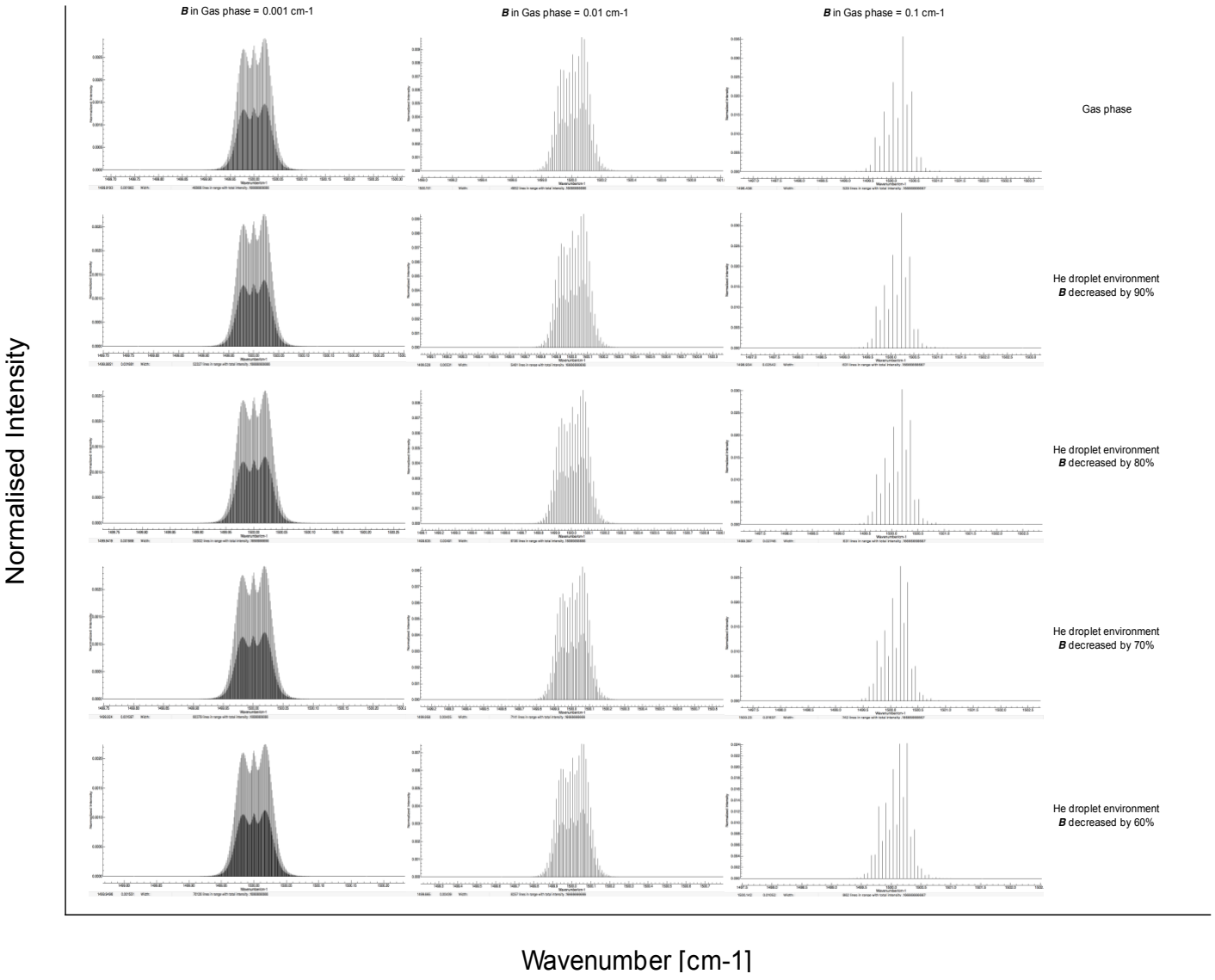

Fig. 4.7a Simulated spectra of field-free symmetric-top rotors with the rotational constant value in gas phase 0.001 cm^{-1}, 0.01 cm^{-1}, and 0.1 cm^{-1}, assuming that the rotational constants in helium environment are reduced 60-90% from their gas phase values

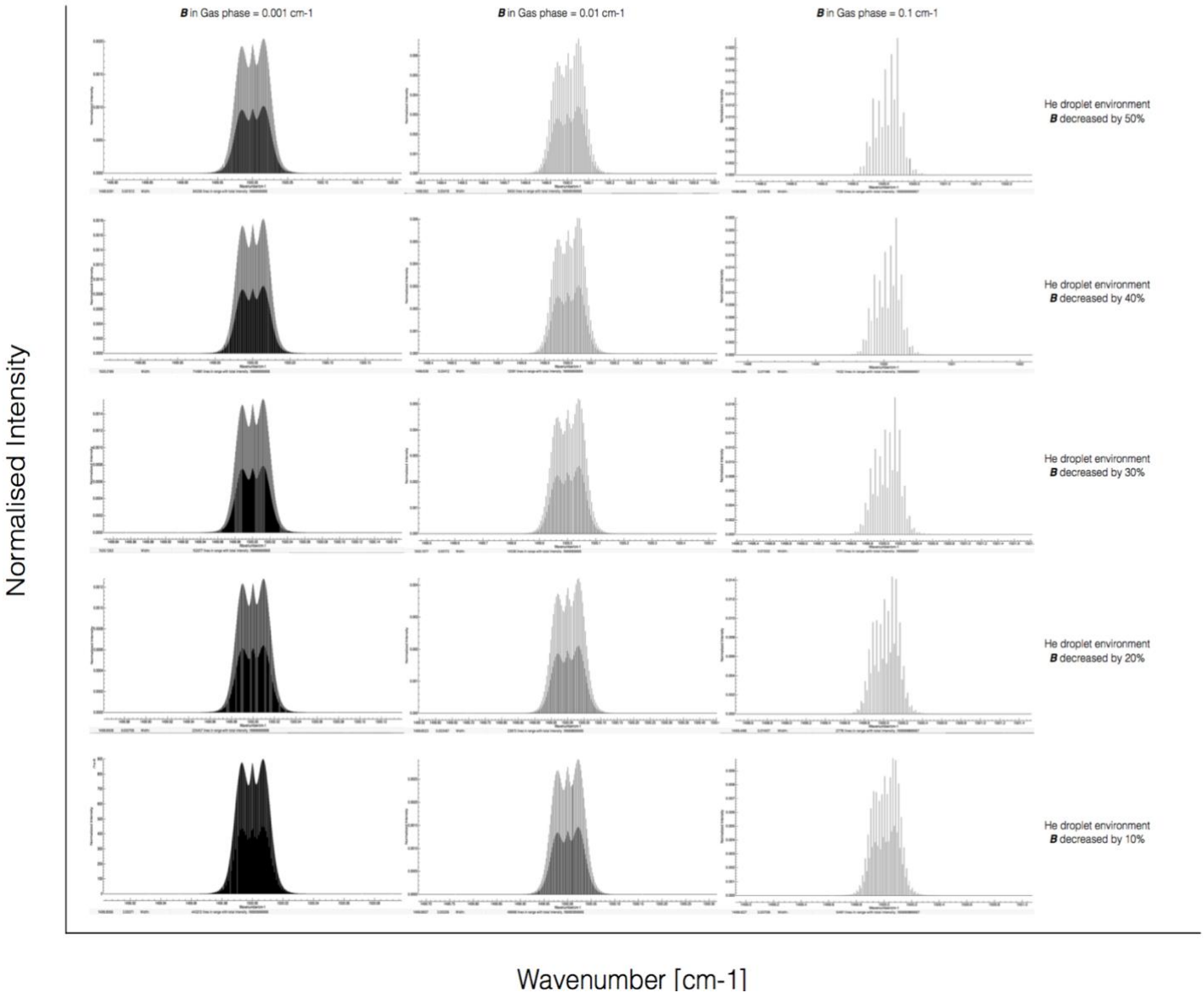

Fig. 4.7b Simulated spectra of field-free symmetric-top rotors with the rotational constant value in gas phase 0.001 cm^{-1}, 0.01 cm^{-1}, and 0.1 cm^{-1}, assuming that the rotational constants in helium environment are reduced 10-50% from their gas phase values

Gas phase				Helium				$\frac{FWHM_{He}}{FWHM_{Gas}}$	$\frac{B_{He}}{B_{Gas}}$
B	C	J-max	FWHM	B	C	J-max	FWHM		
0.001	0.0005	102	0.08248	0.0009	0.00045	108	0.07877	0.95501	0.9
0.001	0.0005	102	0.08248	0.0008	0.0004	109	0.07468	0.90543	0.8
0.001	0.0005	102	0.08248	0.0007	0.00035	116	0.07022	0.85135	0.7
0.001	0.0005	102	0.08248	0.0006	0.0003	125	0.06538	0.79267	0.6
0.001	0.0005	102	0.08248	0.0005	0.00025	137	0.06014	0.72914	0.5
0.001	0.0005	102	0.08248	0.0004	0.0002	160	0.05422	0.65737	0.4
0.001	0.0005	102	0.08248	0.0003	0.00015	184	0.04740	0.57468	0.3
0.001	0.0005	102	0.08248	0.0002	0.0001	224	0.03950	0.47890	0.2
0.001	0.0005	102	0.08248	0.0001	0.00005	314	0.03029	0.36724	0.1
0.01	0.005	33	0.23868	0.009	0.0045	35	0.22838	0.95684	0.9
0.01	0.005	33	0.23868	0.008	0.004	37	0.21699	0.90912	0.8
0.01	0.005	33	0.23868	0.007	0.0035	40	0.20295	0.85030	0.7
0.01	0.005	33	0.23868	0.006	0.003	43	0.18899	0.79181	0.6
0.01	0.005	33	0.23868	0.005	0.0025	46	0.17386	0.72842	0.5
0.01	0.005	33	0.23868	0.004	0.002	52	0.15666	0.65636	0.4
0.01	0.005	33	0.23868	0.003	0.0015	57	0.13706	0.57424	0.3
0.01	0.005	33	0.23868	0.002	0.001	73	0.11365	0.47616	0.2
0.01	0.005	33	0.23868	0.001	0.0005	102	0.08264	0.34623	0.1
0.1	0.05	11	0.57925	0.09	0.045	12	0.60058	1.03682	0.9
0.1	0.05	11	0.57925	0.08	0.04	12	0.58817	1.01539	0.8
0.1	0.05	11	0.57925	0.07	0.035	13	0.57114	0.98599	0.7
0.1	0.05	11	0.57925	0.06	0.03	14	0.56176	0.96981	0.6
0.1	0.05	11	0.57925	0.05	0.025	16	0.52988	0.91477	0.5
0.1	0.05	11	0.57925	0.04	0.02	18	0.48846	0.84326	0.4
0.1	0.05	11	0.57925	0.03	0.015	20	0.44040	0.76029	0.3
0.1	0.05	11	0.57925	0.02	0.01	25	0.37635	0.64972	0.2
0.1	0.05	11	0.57925	0.01	0.005	35	0.29050	0.50151	0.1

Table 7. Rotational constants in gas phase of symmetric-top rotor and their reduction in helium environment with the corresponding J_{max}

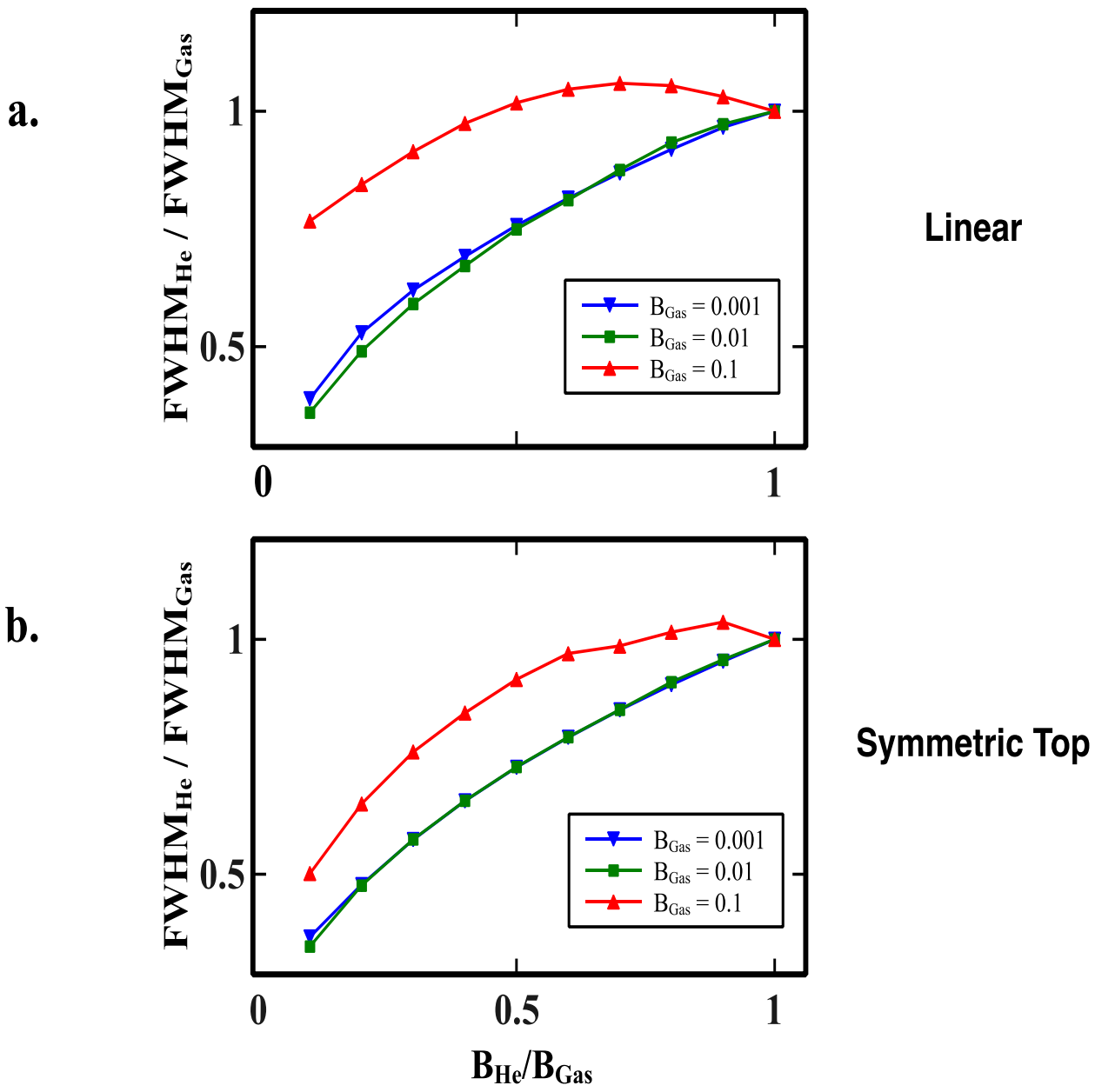

Fig. 4.8 Relative spectral widths plotted against rotational constant renormalization ratios for (a) model linear rotors, and (b) model symmetric top rotors (rotational constant C is taken to be half of B)

From **Fig. 4.8**, we see a relative spectral-width dependence on the rotational constant renormalization ratio to be monotonously increasing for gas phase rotational constants 0.001 cm^{-1} and 0.0.01 cm^{-1}. However for a gas-phase rotational constant of 0.1 cm^{-1}, the scaling is no longer linear for either the linear or the symmetric top case.

4.4 Spectral-width analysis of sample molecules

Encouraged by the monotonous relative spectral-width curves in the models described in the previous two sections, we set out to perform a similar analysis for some actual molecules.

This analysis somewhat differs from the model analysis in sections 4.2 and 4.3 as the values of gas-phase and helium environment rotational constants are taken from experimental literature, while the values of the anisotropy parameter Δ and the dimensionless coupling strength parameter γ, are taken from the supplementary information provided in ref. [23]. The objective was to find a meaningful descriptor gleaned from the properties of a given molecule in the gas-phase and helium environment (such as γ), that correlates with the relative spectral-width. Unfortunately, we report a negative result, in that no such clear dependence could be found. **Fig. 4.9** shows the stick spectra for the investigated molecules (c.f. **Table 1**, from chapter 3).

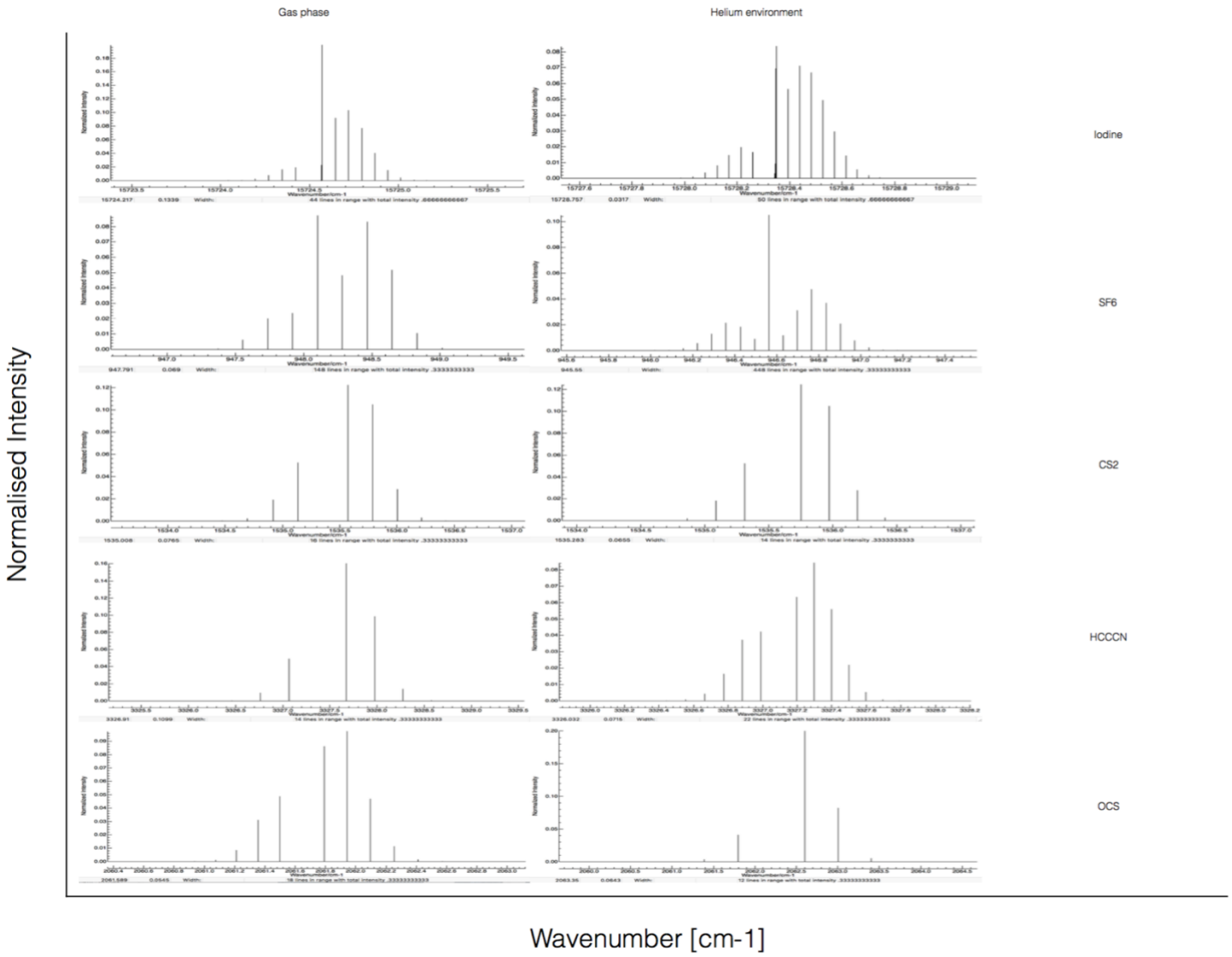

Fig. 4.9a Simulated spectra of field-free sample molecules with their corresponding rotational constant in gas phase and their reduced rotational constant in helium nanodroplet environment

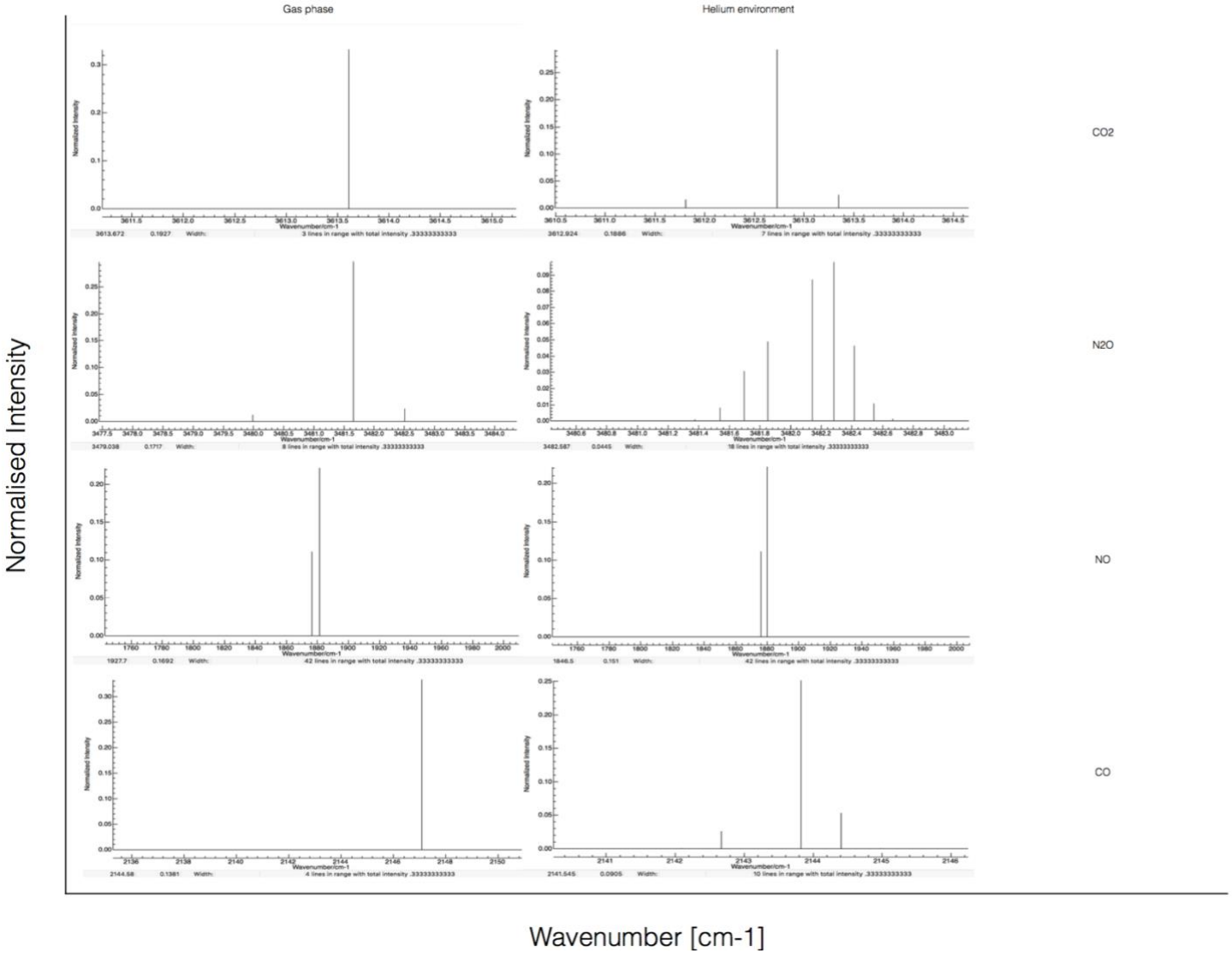

Fig. 4.9b Simulated spectra of field-free sample molecules with their corresponding rotational constant in gas phase and their reduced rotational constant in helium nanodroplet environment

Molecule	Gasphase		Helium		γ	Δ	$\frac{FWHM_{He}}{FWHM_{Gas}}$	$\frac{B_{He}}{B_{Gas}}$
	B	FWHM	B	FWHM				
OCS	0.20164	0.14001	0.07442	0.36130	0.0311	-	2.58052	0.369074
SF_6	0.09108	0.16073	0.03396	0.40110	0.0145	6.28	2.49548	0.372843
N_2O	0.41378	0.14001	0.0742	0.33560	0.0378	-	2.39697	0.179322
HCCCN	0.15163	0.14004	0.05173	0.2974	0.0217	6.97	2.12417	0.3411
CO_2	0.38750	0.14000	0.154	0.14001	0.0545	7.16	1.00007	0.3974
HF	20.5602	0.14002	20.2518	0.14002	3.26	6.07	1	0.98500
NH_3	9.9466	1.2181	7.5	1.2181	1.71	5.78	1	0.754027
HCN	1.47822	0.14005	1.2045	0.14002	0.399	-	0.99978	0.81483
CO	1.9190	0.14005	0.2895	0.14001	0.491	-	0.99971	0.15086
HCl	10.44	0.14017	0.31	0.14001	2.23	4.54	0.99885	0.02969
CH_4	5.256	0.10103	5.012	0.10090	1.37	3.83	0.99871	0.95357
CS_2	0.10912	0.14535	0,.11132	0.14419	0.0156	6.97	0.99201	1.020123
NO	1.67195	7.3044	1.253	6.3585	0.874	1.89	0.87050	0.74942
I_2	0.03731	0.25709	0.02242	0.21710	0.0159	2.35	0.84445	0.60085

Table 8. Rotational constants in gas phase and helium environment of sample molecules (in cm^{-1}) with their corresponding anisotropy parameter Δ (in cm^{-1}), dimensionless coupling strength parameter $\boldsymbol{\gamma}$, and relative spectral width.

4.5 Conclusions

It has been corroborated in this thesis that PGOPHER (version 10.0.505) is capable of reproducing spectra found in the literature and therefore can be relied upon as providing valid spectral simulations.

The main result of this thesis is the correlation between the relative spectral width and the renormalization ratio for the rotational constant. For small B, the spectral width is found to increase linearly with the renormalization ratio. This scaling behavior, however, is found to be different for large rotational constants, where the corresponding red curves pertaining to both and symmetric top rotors become non-linear, see **Fig. 4.8.**

The failure to find a similar scaling behavior in actual molecules (listed in **Table 8**) is not completely surprising, considering that the rotational constants of most of these molecules exceed 0.1 cm^{-1} - the regime in which the scaling becomes non-linear in our model analysis. It would be interesting to perform the same study on actual molecules whose rotational constants are an order of magnitude or two smaller than the ones presented in **Table 8**. Large organic molecules such as phthalocyanine-based systems, porphyrins, anthracene and tetracene, all of which have been investigated in both the gas-phase and Helium environment [50-56], would be more amenable to establishing the dependence that was hoped for in this study. The lack of the anisotropy parameter (Δ) values for these molecules (which depends on extensive ab initio calculations for the dopant-He PES), and hence the dimensionless coupling strengths (γ), prevented us from extending the study to those systems. It is hoped that at some point in the future, these values would become available, in addition to an upgraded angulon formalism for symmetric and asymmetric tops through joint efforts of the Friedrich and Lemeshko groups.

A final note: Following the results of Slenczka et. al. [57], the idea of free rotation of the Phthalocyanine molecule in helium nanodroplets has been called into question. A similar dependence study comparing experimental spectral-widths of the organic molecules mentioned above, in the gas-phase and helium droplets, obtained from high-resolution electronic spectroscopy could throw added light on the entire issue, and complement the theoretical analyses.

References

[1] R. Lehnig, M. Slipchenko, S. Kuma, T. Momose, B. Sartakov, and A. Vilesov, J. Chem. Phys. **121**, 9396 (2004).

[2] J. P. Toennies and A. F. Vilesov, Annu. Rev. Phys. Chem. **49**, 1 (1998).

[3] K. Callegari, K. K. Lehmann, R. Schmied, and G. Scoles, J. Chem. Phys. **115**, 10090 (2001).

[4] F. Stienkemeier and A. F. Vilesov, J. Chem. Phys. **115**, 10119 (2001).

[5] J. P. Toennies and A. F. Vilesov, Angew. Chem. **43**, 2622 (2004) .

[6] D. R. Tilley and J. Tilley, *Superfluidity and Superconductivity* (Institute of Physics Publ., Bristol, 1990).

[7] J. Wilks and D. S. Betts, *An Introduction to Liquid Helium* (Calendon, Oxford, 1987)

[8] C.M. Western, *Journal 222 of Quantitative Spectroscopy & Radiative Transfer*, **186**, 221–242 (2017).

[9] G. N. Zastenker, E. Salerno, F. Buehler, P. Bochsler, M. Bassi, Yu. N. Agafonov, N. A. Eismont, V.V. Khrapchenkov, and H. Busemann, Astrophysics **45**, 131 (2002).

[10] N. Singh, *Thermodynamical Phase transitions, the mean-field theories, and the renormalization (semi)group: A pedagogical introduction*, 2014.

[11] J. Peter Toennies and Andrey F. Vilesov, Angew. Chem. Int. Ed. **43**, 2622 – 2648, (2004).

[12] Eva-Maria Wirths, *High Resolution Electronic Spectroscopy of van der Waals Clusters Formed in Superfluid Helium Nanodroplets*. PhD thesis, Universität Regensburg, 2014.

[13] M. Lewerenz, B. Schilling, J. P. Toennies, J. Chem. Phys. **102**, 8191 (1995).

[14] B. Dick and A. Slenczka, J. Chem. Phys., **115**, 10206 (2001).

[15] K. Szalewicz, Int. Rev. Phys. Chem. **27**, 273 (2008).

[16] S. Grebenev, M. Hartmann, M. Havenith, B. Sartakov, J. P. Toennies, and A. F. Vilesov, J. Chem. Phys. **112**, 4485 (2000).

[17] C. Callegari, A. Conjusteau, I. Reinhard, K. K. Lehmann, G. Scoles, and F. Dalfovo, Phys. Rev. Lett. **83**, 5058 (1999).

[18] C. Callegari, A. Conjusteau, I. Reinhard, K. K. Lehmann, G. Scoles, and F. Dalfovo, Phys. Rev. Lett. **84**, 1848 (2000).

[19] K. K. Lehmann, J. Chem. Phys. **114**, 4643 (2001).

[20] K. K. Lehmann, J. Chem. Phys. **117**, 1595 (2002).

[21] M. V. Patel, A. Viel, F. Paesani, P. Huang, and K. B. Whaley, J. Chem. Phys. **118**, 5011 (2003).

[22] CRC handbook of chemistry and physics, 70th ed., edited by R. C. Weast (CRC Press, Boca Raton, FL, 1990).

[23] M. Lemeshko, Phys. Rev. Lett. **118**, 095301 (2017).

[24] L. Tisza, Nature 141, 913 (1938).

[25] F. London, Nature, 141, 643 (1938).

[26] O.Svelto, *Principles of Lasers*, 5th Edition, Springers, New York, 2010, **34-39.**

[27] C. Callegari, I. Reinhard, K. K. Lehmann, G. Scoles, K. Nauta, and R. E. Miller, J. Chem. Phys. **113**, 4636 (2000).

[28] P.L. Stiles, K. Nauta, and Roger E. Miller, Phys. Rev. Lett. **90**, 135301(2003).

[29] S. Grebenev, M. Hartmann, M. Havenith, B. Sartakov, J.P. Toennies, and A.F. Vilesov, J. Chem. Phys. **112**, 4485 (2000).

[30] K. Nauta and R. E. Miller, Phys. Rev. Lett. **82**, 4480 (1999).

[31] D. Blume, M. Lewerenz, F. Huisken, and M. Kaloudis, J. Chem. Phys. **105**, 8666 (1996).

[32] K. Nauta and R. E. Miller, J. Chem. Phys. **113**, 9466 (2000).

[33] M. Behrens, U. Buck, R. Fröchtenicht, M. Hartmann, F. Huisken, and F. Rohmund , J. Chem. Phys. **109**, 5914 (1998).

[34] K. Nauta and R. E. Miller, in Atomic and molecular beams: The state of the art 2000, edited by R. Campargue (Springer Verlag, Berlin, 2001), part VI.3, p. 775.

[35] Nikolas Pörtner, J. Peter Toennies, and Andrej F. Vilesov, J. Chem. Physics **117**, 6054 (2002).

[36] J.I. Steinfeld, R. N. Zare, L. Jones, M. Lesk, and W. Klemperer, J. Chem. Physics **42**, 25-33 (1965).

[37] M. Gutmann, D. M. Willberg, and A. H. Zewail, J. Chem. Physics **97**, 8037 (1992).

[38] Álvaro Valdés, Rita Prosmiti, Pablo Villarreal, Gerardo Delgado-Barrio, and Hans-Joachim Werner, J. Chem. Physics **126**, 204301 (2007).

[39] M. Hartmann, R. E. Miller, J. P. Toennies, and A. Vilesov, Phys. Rev. Lett. **75**, 1566 (1995).

[40] J. S. Wells, M. Schneider, A.G. Maki, J. Mol. *Spectrosc.***132**, 422-428 (1988).
[41] F. Mivehvar, Clément Lauzin, A.R.W. McKellar, N. Moazzen-Ahmadi, J. Mol. *Spectrosc.* **281**, 24-27 (2012).
[42] K. Nauta, and R. E. Miller, J. Chem. Physics **115**, 10254 (2001).
[43] K. von Haeften, A. Metzelthin, S. Rudolph, V. Staemmler, and M. Havenith, Phys. Rev. Lett. **95**, 215301 (2005).
[44] L. A. Surin, A. V. Potapov, B. S. Dumesh, S. Schlemmer, Y. Xu, P. L. Raston, and W. Jäger, Phys. Rev. Lett. **101**, 233401 (2008).
[45] Claudio E. Chuaqui, Robert J. Le Roy, and A. R. W. McKellar, J. Chem. Physics **101**, 39 (1994).
[46] D. H. Rank, B.S. Rao, and T. A. Wiggins, J. Mol. *Spectrosc.* **17,** 122-130 (1965).
[47] G. Murdachaew, K. Szalewicz, H. Jiang, and Z. Bačić, J. Chem. Physics **121**, 11839 (2004).
[48] M. H. Alexander, B. Pouilly, T. Duhoo, J. Chem. Phys. **99**, 1752 (1993).
[49] K. Nauta and R.E. Miller, Chemical Physics Letters **350**, 225-232 (2001).
[50] A. Slenczka, B. Dick, M. Hartmann, and J. P. Toennies, J. Chem. Phys. **115**, 10199-10205 (2001).
[51] Dominik Pentlehner, Ricarda Riechers, Bernhard Dick, Alkwin Slenczka, Uzi Even, Nachum Lavie, Ravie Brown, and Kfir Luria. Rapidly pulsed helium droplet source. Rev. Sci. Instrum., 80:043302 – 1 – 9 (2009).
[52] S. Krasnokutski, G. Rouillé, and F. Huisken, Chemical Physics Letters, **406**, 386-392 (2005).
[53] Martin C. R. Cockett and Katsumi Kimura, J. Chem. Phys., **100**, 3429 – 3441 (1994).
[54] W. R. Lambert, P. M. Felker, J. A. Syage, and A. H. Zewail, J. Chem. Phys., **81**, 2195 – 2208, (1984).
[55] Ricarda Eva Friederike Elisabeth Riechers, *High-resolution spectroscopy in superfluid helium droplets. Investigation of vibrational fine structures in electronic spectra of phthalocyanine and porphyrin derivatives.* PhD thesis, Universität Regensburg, 2011.
[56] H.D. Whitley, J.L. DuBois, and K.B. Whaley, The Journal of Chemical Physics **131**, 124514 (2009).

[57] S. Fuchs, J. Fischer, A. Slenczka, M. Karra, B. Friedrich, *Microsolvation of phthalocyanine molecules in superfluid helium nanodroplets as revealed by the optical line shape at the electronic origin* (2018) - **arXiv:1801.03679**

Thanks

I would like to thank Prof. Dr. Bretislav Friedrich, for all of the help and kindness that he has shown me, especially for welcoming me very warmly at *The Fritz-Haber Institute* of the Max Planck Society. He has given me so much time in the midst of his busyness, to give me suggestions and to help me improve my Bachelor thesis.

I also want to thank Mallkarjun Karra, who helped me to understand various theories by giving me many inspiring publications to read, and for answering my questions. He has helped me by giving many ideas, particularly in using *Keynote* on Mac to create and arrange many figures in one paper.

Lastly, I want to say thanks to Prof. Dr. Beate Paulus, for her willingness to give her time in supervising and grading this thesis.

Erklärung

Hiermit versichere ich, dass ich die vorliegende Arbeit selbständig verfasst und keine anderen als die angegebenen Quellen und Hilfsmittel benutzt habe, dass alle Stellen der Arbeit, die wörtlich oder sinngemäß aus anderen Quellen übernommen wurden, als solche kenntlich gemacht worden sind, und dass die Arbeit in gleicher oder ähnlicher Form noch keiner anderen Prüfungsbehörde vorgelegt wurde.

Berlin, den 25. Februar 2018